Switching of macromolecular ligand display by thermoresponsive polymers mediates endocytosis of multi-conjugate nanoparticles.

Edward J Sayers,[#1] Johannes P Magnusson,[#2] Paul R Moody,[1] Francesca Mastrotto,[2,3] Claudia Conte,[2] Chiara Brazzale,[3], Paola Borri,[4] Paolo Caliceti,[3] Peter Watson,[4] Giuseppe Mantovani,[2] Jonathan Aylott,[2] Stefano Salmaso,[3] Arwyn T Jones[1] and Cameron Alexander*[2].*

[1]Cardiff School of Pharmacy and Pharmaceutical Sciences, Cardiff University, Redwood Building, King Edward VII Ave, Cardiff CF10 3NB, United Kingdom.

[2]School of Pharmacy, University of Nottingham, University Park, Nottingham, NG72RD, United Kingdom.

[3]Department of Pharmaceutical and Pharmacological Sciences, University of Padova, Via Marzolo, 5 – 35131, Padova, Italy.

[4]School of Biosciences, Cardiff University, The Sir Martin Evans Building, Museum Avenue, Cardiff, CF10 3AX, United Kingdom..

ABSTRACT

Ligand-mediated targeting and internalization of plasma membrane receptors is central to cellular function. These types of receptors have accordingly been investigated as targets to facilitate entry of diagnostic and therapeutic constructs into cells. However, there remains a need to characterize how receptor targeting agents on nanoparticles interact at surface receptors and whether it is possible to control these interactions via exogenous stimuli. Here, we describe the switchable display of the iron-transporting protein, transferrin (Tf), at the surface of thermoresponsive polymer-coated gold nanoparticles, and show that internalization of the coated nanoparticles into target cells changes across temperature ranges over which transferrin is expected to be sterically 'hidden' by an extended polymer chain and then 'revealed' by polymer chain collapse. The switching process is dependent on the numbers of transferrin molecules and thermoresponsive polymer chains attached, and whether the assay temperature is above or below the transition temperatures of the responsive polymers at the nanoparticle surfaces. Significantly, however, the control of internalization is critically reliant on overall nanoparticle colloidal stability while the thermoresponsive component of the surface undergoes conformational change. The data show that the cell entry function of complex and large biomolecule ligands can be modulated by polymer-induced accessibility change, but that a simple 'hide and reveal' mechanism for ligand display following polymer chain collapse is insufficient to account for nanoparticle uptake and subsequent intracellular trafficking.

Introduction

Polymer-metal hybrid nanoparticles offer many advantages for diagnosis and therapy, owing to the possibility to endow these materials with multiple functionalities for detecting disease, releasing therapeutic agents or treat the pathology by enhancing externally applied physical stimuli.[1-6] However, the clinical applications of nanoparticles in general have been limited by

complex and unpredictable pharmacokinetics and targeting.[7-10] In order to achieve maximal clinical response *in vivo* any diagnostic or therapeutic agent needs to accumulate at the target tissue and gain access to disease relevant cells and appropriate intracellular compartments. Even if a nanoparticle can successfully transit across *in vivo* barriers such as mucosal surfaces or plasma membranes, successful internalization at a specific desired cell requires spatial and temporal display of a functional signal, such as a ligand, to interact with a cellular receptor. Maintaining this ligand accessibility has proven to be challenging owing to the difficulties in ensuring that synthetic materials accurately display their functionality in complex biological environments.[11-14]

Amongst the emerging sets of materials for therapeutic delivery and diagnostic applications *in vivo* are gold nanoparticles (AuNPs) and their derivatives.[15-18] These systems are of significant interest because methods to modulate surface functionality, particle charge, topology, shape and size, as well as simple routes to multiple different surface chemistries, are very well-established for AuNPs. As a consequence, AuNPs are promising test-beds for probing structure-function relationships in biomedical settings, especially as key chemical parameters and material properties can be altered systematically in order to assess their effects on biological activity. Ligand display is particularly amenable to control at AuNP surfaces because of well-defined and robust conjugation approaches developed so far; in fact many α,ω-heterobifunctional thiol reagents are commercially available, allowing strong covalent attachment in defined domains to the gold substrate and providing chemical handles to attach biological ligands.

The range of ligands attached to AuNPs which have been used to influence cellular interactions includes small molecule agents, peptides, growth factor derivatives and proteins.[12, 19-23] High molecular weight ligands such as proteins offer high recognition selectivity with their cognate receptors under tightly-defined conditions and so are obvious candidates to target

AuNPs to specific receptors on cells of interest. The iron binding protein transferrin (Tf), has been extensively studied as a delivery vector for specific therapeutics which otherwise show limited cellular uptake.[24-28] This is because transferrin plays an essential role in the transport of free iron into cells, its mechanism of uptake is well established, it is constitutively endocytosed and transferrin receptors (TfR) are overexpressed in a number of disease states. Tf-drug conjugates have been used to target solid tumors owing to the requirements of some cancer cells for high levels of iron. However, ligand-mediated endocytosis, as a single method of targeting, has limitations owing to the presence of receptors in healthy tissue, and this is a particular issue for Tf-based systems, as transferrin receptors are also highly expressed at the blood brain barrier.[25] It would therefore be very desirable if it were possible to 'hide' ligands such as Tf from cognate receptors on healthy cells, but display the protein when in proximity to diseased tissue, thus controlling the functionality of Tf-targeted diagnostics and therapeutics to specific disease sites.

Here we describe how Tf-mediated endocytosis can be switched by controlling the display of the protein at gold nanoparticle surfaces utilizing multicomponent polymer-transferrin gold nanoparticle conjugates. We synthesized gold particles functionalized with charge- and entropically-stabilizing zwitterionic hydrophilic polymers containing azide and thiol termini. Transferrin and thermoresponsive polymers were subsequently attached to the polymer-AuNP conjugate via dibenzocyclooctyne (DBCO) copper-free click chemistry. The physical properties of nanoparticles with a range of different Tf and thermoresponsive polymer grafting densities were measured and their effects on cellular transport evaluated. The AuNP polymer protein conjugates synthesized were colloidally stable over the time course of the cellular uptake experiments. Temperature-mediated uptake of the thermoresponsive AuNP Tf conjugates was achieved via selection and screening of different polymer and protein grafting densities.

Shielding of Tf via the chain-extended responsive polymers resulted in low levels of cell entry at 37 °C, whereas chain-collapse of polymers at temperatures relevant to clinically applied ultrasound and local tumour hyperthermia (39-41 °C),[29] resulted in enhanced nanoparticle uptake. This demonstrated that a macromolecular ligand for a cell surface receptor could be 'switched on' or 'off' by an external stimulus. In addition, confocal microscopy analysis of the multi-conjugate AuNPs in a cancer cell line demonstrated that transport occurred rapidly to lysosomal compartments.

RESULTS

Preparation of gold nanoparticles, polymers and polymer-protein-conjugates

Gold nanoparticle protein polymer conjugates were prepared by successive synthesis and coupling of the individual gold, polymer and protein components. The first step involved anchoring an ATRP-type initiator (Compound **1**, Figure 1a) derived from readily available lipoic acid, to gold nanoparticles, using the cyclic disulfide terminus from the lipoic acid to form strong bonds to the metal surface.

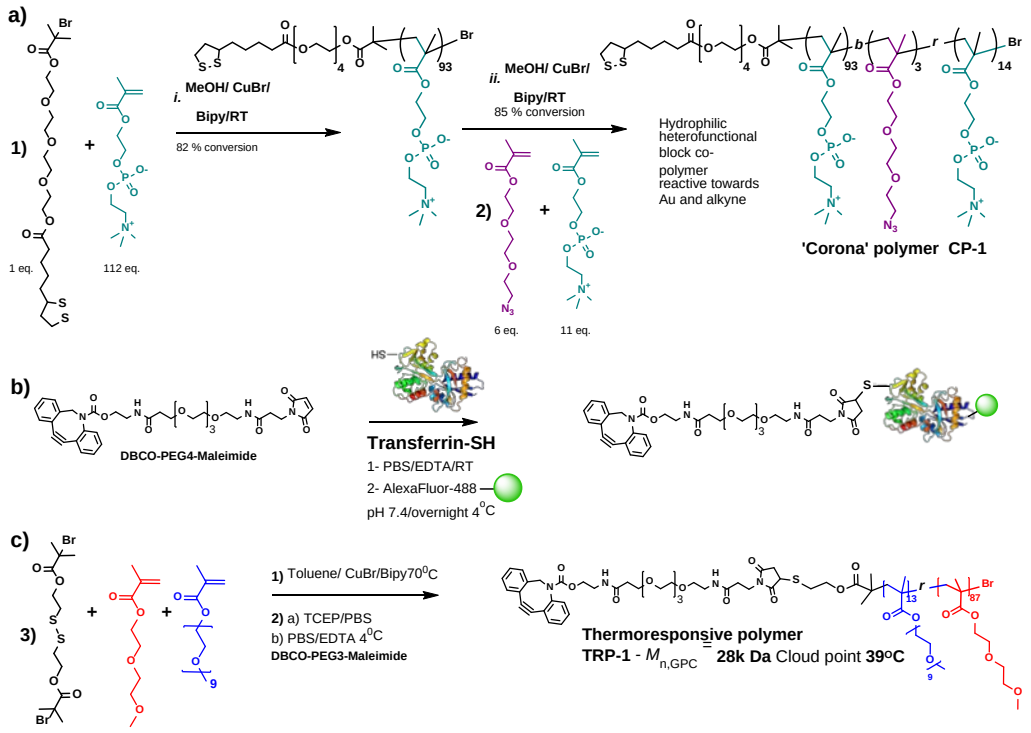

Figure 1: Synthesis overview: a) Hydrophilic MPC-azide-TriEG-functional block-copolymer for AuNP (lipoic acid ester) primary corona; b) Thiotransferrin DBCO conjugation and Alexa Fluor 488 labelling; c) Thermoresponsive PEGMA DBCO functionalized polymer. The co-monomer ratios in CP-1 were estimated from NMR spectra integrals and indicate actual content as opposed to estimates from co-monomer addition ratios.

Gold nanoparticles were synthesized by *in situ* reduction of gold salts and characterized by TEM (Figure S1). Average diameters of the AuNPs were 25-30 nm (TEM) prior to polymer conjugation. From compound (**1**), a 2-methacryloyloxyethyl phosphorylcholine (MPC) homopolymer was initially grown. At high MPC conversion (DP ~92), 2-(2-(2-azidoethoxy)ethoxy)ethyl methacrylate monomer (**2,** Azido-TriEG-Methacrylate) and an additional amount of the MPC monomer were added to form the final MPC-azide-TriEG block-copolymer. NMR analysis of the purified resulting block-copolymer revealed that each MPC-azide-TriEG copolymer contained an average of 3 azide functional side-chains.

Thio-transferrin, a Tf mutant with a free cysteine,[29, 30] was used to synthesize the reactive alkyne DBCO Tf derivative (Figure 1b). DBCO–maleimide was added to the thio-transferrin in slight excess, resulting in Tf conjugation of 70% efficiency: increases in the molar equivalent of maleimide-DBCO linker to Tf did not improve the conjugation to thiol. The partially DBCO-modified Tf proved difficult to purify at this stage, but was found to be suitable for subsequent coupling reactions since the unmodified protein was nonreactive towards the AuNP MPC-azide conjugates and was easily removed after nanoparticle conjugation. The DBCO-Tf conjugate was labelled with Alexa Fluor 488 (AF488) SDP to allow monitoring of nanoparticle uptake and localization of the transferrin-gold nanoparticle conjugates into cells. Spectroscopic analysis after GPC removal of the free dye demonstrated that on average 2.7 dye molecules were linked to the DBCO-Tf.

For thermal modulation of transferrin accessibility at the AuNP surfaces, we aimed to attach polymers based on thermoresponsive polyethylene glycol methacrylate (pPEGMA)[30] to form a 'reversibly shielding' outermost layer. Accordingly, the pPEGMA materials were prepared from a disulfide bifunctional initiator (Figure 1c), with co-monomers chosen to control the onset of coil-to-globule transitions to around 37 °C, and molar masses varied to modulate steric hindrance. The resultant disulfide-linked co-polymers were readily cleaved using TCEP to produce polymer chains with free thiol termini, which in turn were reacted with DBCO - maleimide and purified by Gel Permeation Chromatography (GPC) to afford an alkyne-functional thermoresponsive polymer (coded TRP-1, Table 1), designed to react with the azide side-chains on the MPC- azido-TriEG co-polymers already attached to gold nanoparticle substrates. The cleavage of the disulfide bond in the 'dimeric' pPEGMA material and subsequent reaction of the pPEGMA-thiol terminus with DBCO-maleimide to form a reactive alkyne (TRP-1 Figure 1) were monitored by Ellman assays and GPC analysis to ensure

completion of reaction. The properties of the zwitterionic MPC 'corona' polymer (CP-1) and the thermoresponsive polymers (TRP-1 Figure 1) are shown in Table 1 and Figure S2 (ESI).

Polymer	M_n[a] / kDa	M_n / kDa GPC	M_w/M_n	Cloud point °C
Azide-TriEG-MPC	31.7	26[b]	1.2	-
TRP-1 (pPEGMA-DBCO)	27.9	25 [c]	1.6	39[d]

Table 1: Polymer characteristics. a) Theoretical, calculated from monomer/initiator ratio and conversion. b) From GPC (DPBS, PEG standards); c) From GPC ($CHCl_3$, polystyrene standards); d) measured at 1.25 $mg.mL^{-1}$ in PBS.

Synthesis and characterization of AuNP polymer-protein conjugates

Functionalization of the AuNPs with the MPC-azide-polymer via the lipoic disulfide group occurred rapidly simply by mixing in aqueous solutions. Any unreacted polymer was removed by centrifugation of the nanoparticles and removal of the supernatant. Grafting density was determined by measuring residual non-conjugated MPC polymer in the supernatant; GPC analysis of this solution revealed that approximately 500 polymer chains were attached to each gold nanoparticle, in accord with similar grafting densities reported for AuNPs of similar sizes previously.[31, 32] Particle recovery after repeated centrifugation and purification cycles was essentially quantitative, i.e. no macro particle aggregation, nor any shift in the UV absorption spectrum for the particles was observed. Centrifugal analysis of the polymer-functionalized gold nanoparticles showed decreased sedimentation speed in comparison to the unmodified gold nanoparticles (data not shown). The polymer functionalized gold nanoparticles were

stable in isotonic phosphate buffered saline and cell culture media while the unmodified gold nanoparticles aggregated rapidly in the presence of salt.

Transferrin DBCO-AF488 conjugates were grafted onto the MPC-azide functionalized AuNPs to generate batches containing grafting ratios of 2, 4 or 8 transferrin equivalents. After reaction at 4°C with gentle agitation for three days, the resultant Tf-AuNP conjugates were repeatedly isolated by centrifugation and resuspension in buffer solutions until no free protein was detected in the supernatant. Particle concentrations were confirmed by UV-Vis spectroscopy and particle recovery was calculated by direct comparison to the initial stock AuNP MPC-azide solution. Protein grafting density was determined by comparing the AF488 fluorescence in the initial supernatant to that of the protein AF488 stock. Recovery of the initial nanoparticle stock concentration ranged from 92.5% to 99% for all three batches.

The DBCO-functionalized thermoresponsive polymer TRP-1 was grafted directly onto the three Tf-AuNP conjugates by adding large excesses (100 equivalents of TRP-1 with respect to azide groups on the NPs) for each AuNP per batch. The particulate suspensions were allowed to react for three days at 4°C. The unreacted polymers were then removed by centrifugation and grafting densities were determined by GPC polymer analysis of the initial supernatants. Centrifugation was repeated until no free polymer was detected in the supernatant. In contrast to the AuNPs with only the zwitterionic MPC-Tf outer surface, addition of the pPEGMA TRP-1 layer caused a significant loss during the purification stages. In each batch around one third of the initial particle content was lost due to irreversible aggregation and adsorption onto the centrifugation tubes. GPC analysis of the supernatant from the batches of the AuNPs with varying Tf content revealed that thermoresponsive polymer grafting increased as the amount of transferrin on the surface of the particle decreased. For the batch of AuNP which had the lowest amount of transferrin attached, an average of 7 pPEGMA TRP-1 chains were conjugated

to each AuNP, while for the batch containing the highest amount of transferrin per AuNP only 2 TRP-1 chains were coupled.

The colloidal stability of the three Tf-AuNP batches with (pPEGMA-Tf-AuNP-1-3) and without (Tf-AuNP-1-3) the pPEGMA outer layer was tested at 37°C in cell culture medium to ensure the particles were stable over the time course of any subsequent cell uptake experiments (Figure S3). Without the pPEGMA corona no aggregation was observed for any of the Tf-AuNP batches over the target time period of 4 h (intended cell culture assay time), while for all the pPEGMA conjugates a small decrease in the UV-Vis absorption (~15%) was observed over the same period.. Light scattering analysis of the nanoparticles in dilute phosphate buffer saline at 33 °C and pH 7.4 showed hydrodynamic diameters of 48-50 nm for the Tf-AuNPs and 55-60 nm for the pPEGMA-AuNPs (Table S1: DLS data based on the number distributions). These sizes were larger than those recorded in TEM (Figure S2), as expected based on the normal drop in sizes recorded for hydrated materials when subject to vacuum dehydration as part of processing for TEM.

Increase in temperature to 41°C, i.e. above the phase transition temperature of the responsive polymer coat for the pPEGMA-Tf-AuNPs, indicated that the particle size distributions were all shifted to higher diameter. Particles with diameters of 60-80 nm were present in all the samples, but also some much larger species (> 300 nm) were apparent in DLS at the higher temperatures, due most likely to protein induced particle association as well as hydrophobic interchain interactions of the pPEGMA grafts (Table S1). The pPEGMA-Tf-AuNP-1 and 2 samples were the most prone to aggregation of the responsive polymer coated materials, whereas pPEGMA-Tf-AuNP-3 particles exhibited much less self-association above the pPEGMA coil-to-globule transition temperature. These differences in nanoparticle aggregation were most likely due to the numbers of pPEGMA chains on the respective nanoparticle outer surfaces, with pPEGMA-Tf-AuNP-1 and 2 samples associating more rapidly with each other due to the presence of

larger hydrophobic domains on their surfaces above the pPEGMA coil-to-globule transition temperature compared to pPEGMA-Tf-AuNP-3

Zeta potential measurements (Table S2) of the Tf-AuNPs and pPEGMA-Tf-AuNPs in dilute phosphate buffer revealed that the charges of all the particulate conjugates were negative (~ -6 to -19 mV) across the temperature range tested (33-41°C). These zeta potentials were in line with expectation since Tf is negatively charged at physiological pH and the zwitterionic polymers were not anticipated to contribute to the overall charge. There was also a marked shift to more negative zeta potential with increasing temperature for all samples except pPEGMA-Tf-AuNP-3, which was also the least negatively charged at the highest temperature, 41°C, which have been associated with buffer ion desorption at increased temperature.

The properties of the AuNPs and their conjugates are provided in Table 2, with cartoon representations of their structures shown in Figure 2.

	Code	Number of Tf/AuNP	Number of attached pPEGMA chains/AuNP)	M_n of attached polymer / kDa
Non-thermoresponsive AuNPs	Tf-AuNP-1	0.7	0	-
	Tf-AuNP-2	1.3	0	-
	Tf-AuNP-3	3.0	0	-
Thermoresponsive AuNPs	pPEGMA-Tf-AuNP-1	0.7	6.8	25
	pPEGMA-Tf-AuNP-2	1.3	4.4	25
	pPEGMA-Tf-AuNP-3	3.0	2.2	25

Table 2 Properties of Polymer Transferrin Gold nanoparticle conjugates.

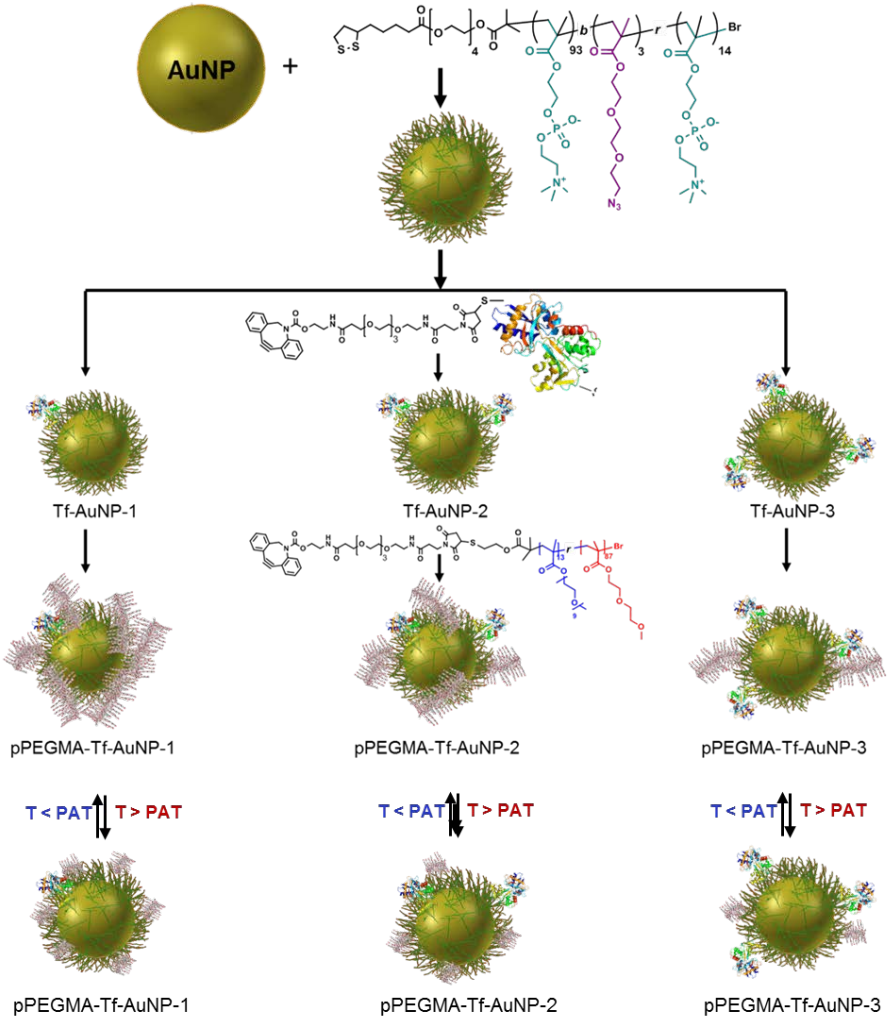

Figure 2. Preparation route, cartoon representations and sample codes for functionalized gold nanoparticles and conjugates. Tf = transferrin, pPEGMA = poly(polyethyleneglycol)methacrylate), AuNP = gold nanoparticle. Tf-AuNP-1 and pPEGMA-Tf-AuNP-1 have a mean of 0.7 Tf per nanoparticle, Au-Tf-NP-2 and pPEGMA-Tf-AuNP-2 have a mean of 1.3 Tf per nanoparticle, and Au-Tf-NP-3 and pPEGMA-Tf-AuNP-3 have a mean of 3.0 Tf per nanoparticle

Biorecognition properties of AuNP polymer-protein conjugates

Surface plasmon resonance (SPR) analysis of the three batches with and without pPEGMA coatings was carried out on an SPR functionalized transferrin receptor (TfR) chip at 25°C and 37°C (Figure S4). These temperatures were chosen to be well below (25°C) and at the point of

onset of the polymer phase transitions (37-39 °C). Control samples of pMPC-AuNP, i.e. the nanoparticles with the passivating poly(zwitterionic) layer but without transferrin or responsive polymer corona were used to evaluate non-specific surface attachment for the SPR measurements. The observed SPR response increased with temperature and with the number of transferrin molecules per AuNP (Figure S4). The addition of the pPEGMA chains to the Tf-AuNP surfaces augmented the binding of the particles to the TfR-functionalised surfaces both at 25°C and 37°C for the pPEGMA-Tf-AuNP-2 (1.3 Tf and 4.4 pPEGMA chains per NP) and pPEGMA-Tf-AuNP-3 (3.0 Tf and 2.2 pPEGMA chains per NP) but decreased with temperature for pPEGMA-AuNP-1 (0.7 Tf and 6.8 pPEGMA per NP). These data (Table 2 and Figure S4) suggested that at the lower Tf content and higher pPEGMA levels, the protein on NPs surface was efficiently sterically hindered from biorecognition on the SPR surfaces. when the thermosensitive polymer was in the extended conformation, whereas with more Tf and fewer pPEGMA chains, there was accessibility to the TfR at the SPR substrate. In addition, the data suggested some non-specific binding to the SPR substrates via the pPEGMA chain, while the lack of adsorption of the pMPC-AuNP particles to the surfaces indicated that the polyzwitterionic layer reduced non-specific adsorption.

The SPR measurements thus showed that the pPEGMA-Tf-AuNPs and their precursors bound to the TfR receptor, i.e. transferrin retained its receptor recognition activity on the surface of the particles, as long as it was accessible. The measurements also confirmed that there were subtle differences between the interactions of the Tf-AuNPs after the addition of the pPEGMA chains and as a function of temperature.

Internalisation studies of AuNP polymer protein conjugates in HeLa cells

Selected AuNP conjugates were evaluated for differences in TfR recognition and endocytic uptake in cells at different temperatures. These experiments were conducted on HeLa cells, as their high expression of transferrin receptors has been well established, and because

intracellular trafficking of proteins and nanoparticles in this cell line has been investigated in depth.[33, 34]

The main hypothesis underlying this study was the possibility for 'switching' particle uptake into cells by hiding the surface-displayed Tf ligands with the pPEGMA layer at temperatures when it was fully hydrated and chain-extended, but revealing the Tf functionality at temperatures at which the pPEGMA chains were expected to be collapsed (see Figure 2). This temperature, based on the Lower Critical Solution Temperature (LCST) of the polymers in solution, is here denoted as aggregation temperature (PAT). Accordingly, live cell imaging confocal microscopy was used to evaluate AuNP uptake at two different temperatures, 33 °C (i.e. below PAT) and 41 °C (above PAT), for non-thermoresponsive Tf-AuNPs-1-3 and thermoresponsive pPEGMA-Tf-AuNP-1-3. HeLa cells were therefore incubated with Tf-AuNPs and pPEGMA-Tf-AuNPs for 2 hours in serum free medium containing 0.1% BSA, washed and imaged immediately (Figure 3). Concentrations were chosen to be low to minimize potential self-association of nanoparticles at temperatures above the polymer PAT. In this way, we aimed to avoid the introduction of another variable – i.e. particle aggregate size, into the analysis of nanoparticle endocytosis, while low concentrations also minimize the possibility of saturating transferrin receptors leading to entry of the NPs into cells via a receptor independent mechanism.

The fluorescence microscopy data for AuNP uptake experiments at 33 °C and 41 °C showed marked enhancement of endocytosis for the thermoresponsive polymer coated particle pPEGMA-Tf-AuNP-3 at temperatures above the expected polymer aggregation temperature (41 °C). The fluorescence from 10 individual images totaling >100 cells was quantified from three independent experiments revealing a significant ($P < 0.005$) 3.6 fold increase in internalization of pPEGMA-Tf-AuNP-3 at 41˚C compared with 33˚C. This enhancement was greater than that observed for AuNPs without the pPEGMA layer (Figure 3). Analysis of the

uptake of Tf alone showed no increase in uptake at 41 °C when compared to 33°C (Supplementary Figure S5) indicating that by increasing the temperature there was no increased rate of Tf endocytosis.

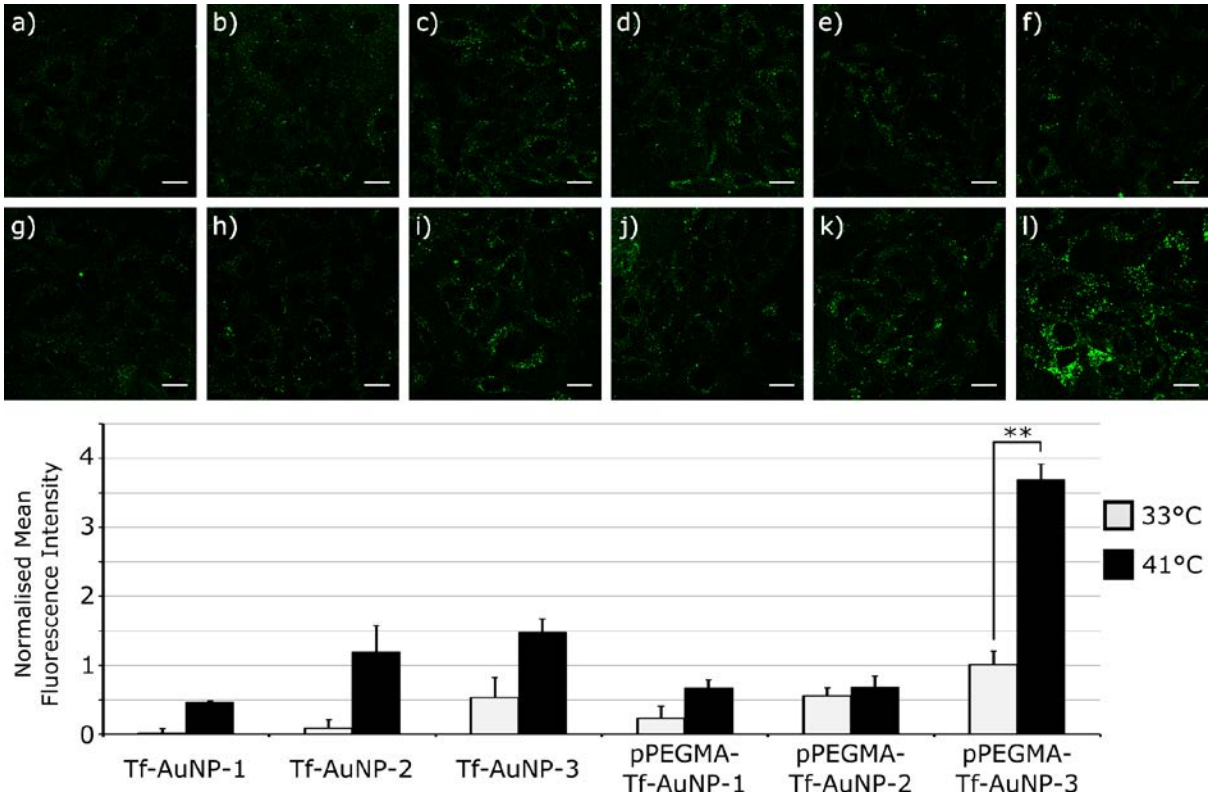

Figure 3: Effect of temperature-on the endocytosis of AuNPs and conjugates in HeLa cells evaluated by confocal microscopy. Images (a-c) and (g-i) show Tf-AuNP-1, -2, -3 at 33 °C and 41 °C, respectively, while images (d-f) and (j-l) show corresponding polymer-coated particles pPEGMA-Tf-AuNP-1, -2, -3 across the same temperature ranges. Scale bars are 20 μm, and the micrographs are all contrast enhanced by the same amount to increase clarity in printed images. Quantification of particle uptake is given in the lower part of the figure, error bars represent standard error from the mean (SEM). Fluorescence intensities from AuNPs were normalized for particle number. The p-value for a t-test between 41 ˚C and 33 ˚C of Tf-AuNP-3 is 0.0036. Fluorescence in images is colored green to represent Alexa488 - original images in b/w in Supporting Information.

These results suggested a polymer-mediated 'switch' of macromolecular receptor-ligand interaction, and its subsequent downstream consequences for particle entry into the targeted cells. The data also suggest that, under the conditions of these assays, too high a ratio of the outer responsive polymer layer to Tf almost completely suppressed particle uptake irrespective of whether the responsive polymer was above or below its PAT. Although pPEGMA-Tf-AuNP-3 nanoparticles were taken up to a four-fold greater extent at a temperature (41 °C) above the polymer aggregation temperature compared to below the PAT, the other nanoparticles in the series, pPEGMA-Tf-AuNP-1 and 2, with higher pPEGMA chain:Tf ratios of ~7 and ~3 (Table 2) were relatively poorly endocytosed even when the polymer chains were collapsed.

In comparison, the uptake of nanoparticles Tf-AuNP-1, Tf-AuNP-2 and Tf-AuNP-3, which did not have responsive polymer coatings, was lower than for the responsive polymer-coated particles at both 33 °C and 41 °C. Zeta potential measurements of the nanoparticles showed that all, irrespective of whether they had a responsive polymer coat, became more negatively charged across the 33 °C and 41 °C range. The pPEGMA-Tf-AuNP-3 particles, which were endocytosed to the highest extent, were less negatively charged than all the other nanoparticles at 41 °C, and aggregated less than the other responsive polymer particles. However, the higher association with cells with these nanoparticles cannot be ascribed to a lower particle repulsion with cells at 41 °C alone, since the zeta potentials of these nanoparticles were similar in value at 37 and 41 °C

Intracellular trafficking of AuNP polymer protein conjugates

The intracellular disposition of the functionalized AuNPs following internalization was then investigated, as display of ligands to cognate receptors and their plasma membrane dynamics also governs intracellular trafficking.[35] We reasoned that Tf would be accessible to the greatest extent for the pPEGMA-Tf-AuNP-3 nanoparticles if the experiments were carried out at 41 °C.

Fluorescently labelled Dextran was pulse chased into HeLa lysosomes, and the cells were subsequently incubated with Tf-AuNPs and pPEGMA-Tf-AuNPs for 2 hours at 41 °C (Figure 4).

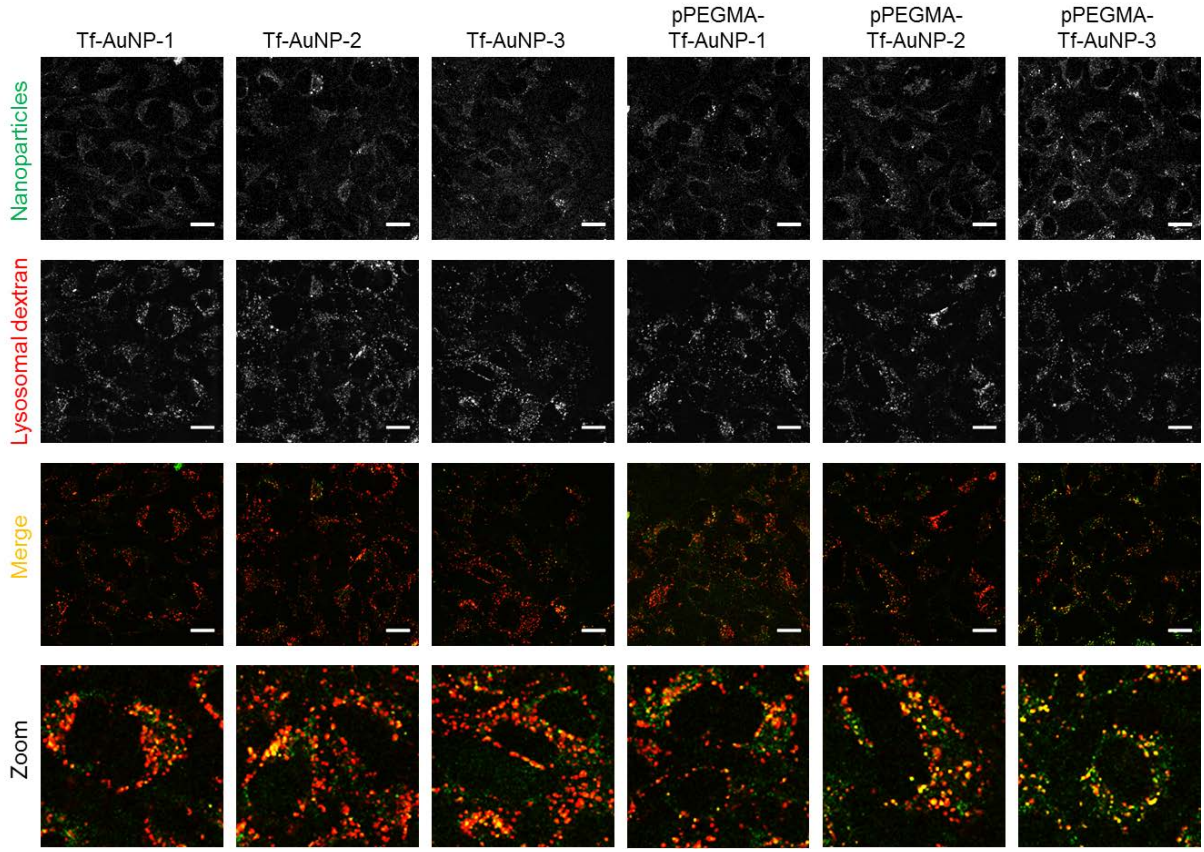

Figure 4: Intracellular localisation of nanoparticles. Lysosomes of HeLa cells were loaded with Dextran-A647(red) by incubating the cells with 100 μg/mL Dextran-A647 for 2 h and chasing overnight in serum containing medium. Cells were incubated with the Tf-AuNPs (green) for 2 h in serum free medium containing BSA at 41°C before being washed and imaged. Images represent single sections, scale bars = 20 μm, and the 'zoomed' micrographs are all contrast enhanced by the same amount to increase clarity in printed images..

As apparent from Figure 4, at this temperature (41 °C), the highest uptake was exhibited by pPEGMA-Tf-AuNP-3, in accord with the prior experiments, but there were no significant differences in the intracellular locations of the nanoparticles, with nanoparticles being associated with the dextran lysosomal marker after 2 hours.

To determine whether pPEGMA-Tf-AuNP-3 was internalized in a Tf receptor-dependent or independent manner we incubated cells with both pPEGMA-Tf-AuNP-3 and a 30-fold excess of unlabeled Tf for 2 hours at 41°C; a temperature at which the Tf proteins attached to the AuNPs were expected to be 'revealed' by collapse of the thermoresponsive polymer (Figure 5). Addition of the free Tf was predicted to out-compete pPEGMA-Tf-AuNP-3 binding to Tf-receptors, and hence reduce internalization of the nanoparticles through a Tf receptor-mediated pathway. Incubation of pPEGMA-Tf-AuNP-3 with excess Tf resulted in a >8 fold decrease in the amount of pPEGMA-Tf-AuNP-3 internalized into the cells over 2hrs. The inhibition of pPEGMA-Tf-AuNP-3 uptake through Tf competition thus confirmed that the main route of internalization of pPEGMA-Tf-AuNP-3 was via the Tf receptor.

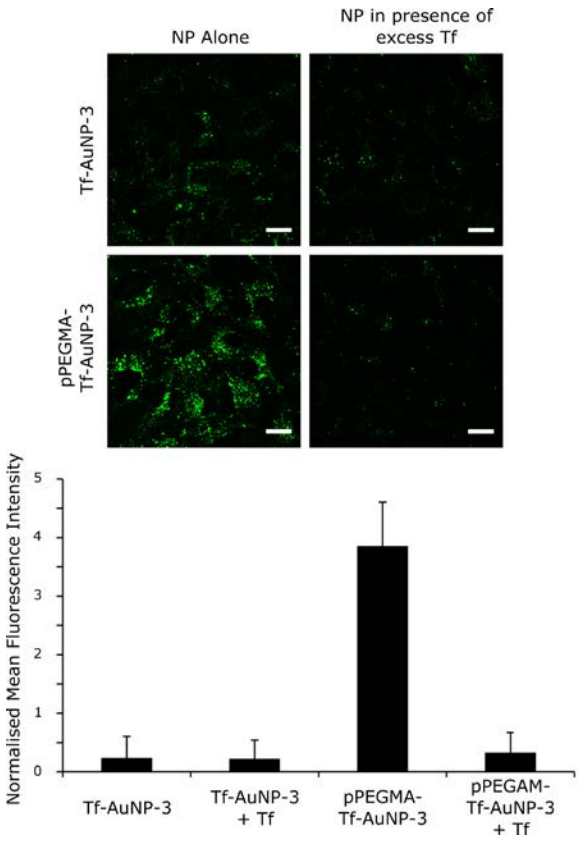

Figure 5: Competition of Tf-AuNP-3 and pPEGMA-Tf-AuNP-3 with excess Tf. HeLa cells were incubated with either Tf-AuNP-3 or pPEGMA-Tf-AuNP-3 in the presence or absence of 625 nM Tf for 2 h in serum free medium containing 0.1% BSA at 41°C before washing and imaging. Representative images are single section confocal micrographs, error bars = 20 μm.

Uptake represents >100 cells from 10 individual images, error bars represent inter-image standard deviation. Fluorescence in images is colored green to represent Alexa488 - original images in b/w in Supporting Information.

Tf-TfR is internalized through clathrin dependent endocytosis; upon reaching the early endosome iron is released and Tf is recycled back to the plasma membrane. Thus, if pPEGMA-Tf-AuNP-3 were to follow the complete Tf pathway, the nanoparticles would be expected to recycle back out of the cell rather than accumulate within. However, we have previously shown that by linking more than one Tf together at the plasma membrane through the use of biotin-streptavidin conjugation, Tf is rerouted to the lysosome rather than recycled from the cell.[35]

We therefore selected the nanoparticle with the highest uptake at 41 °C, pPEGMA-Tf-AuNP-3, and carried out consecutive pulse-chase experiments with dextran-A647 labelled dextran, and in comparison with a fluorescent Tf analogue, Tf-A488 (Figure 6) to assess whether pPEGMA-Tf-AuNP-3 was routed to the lysosome or recycled back out of the cell.

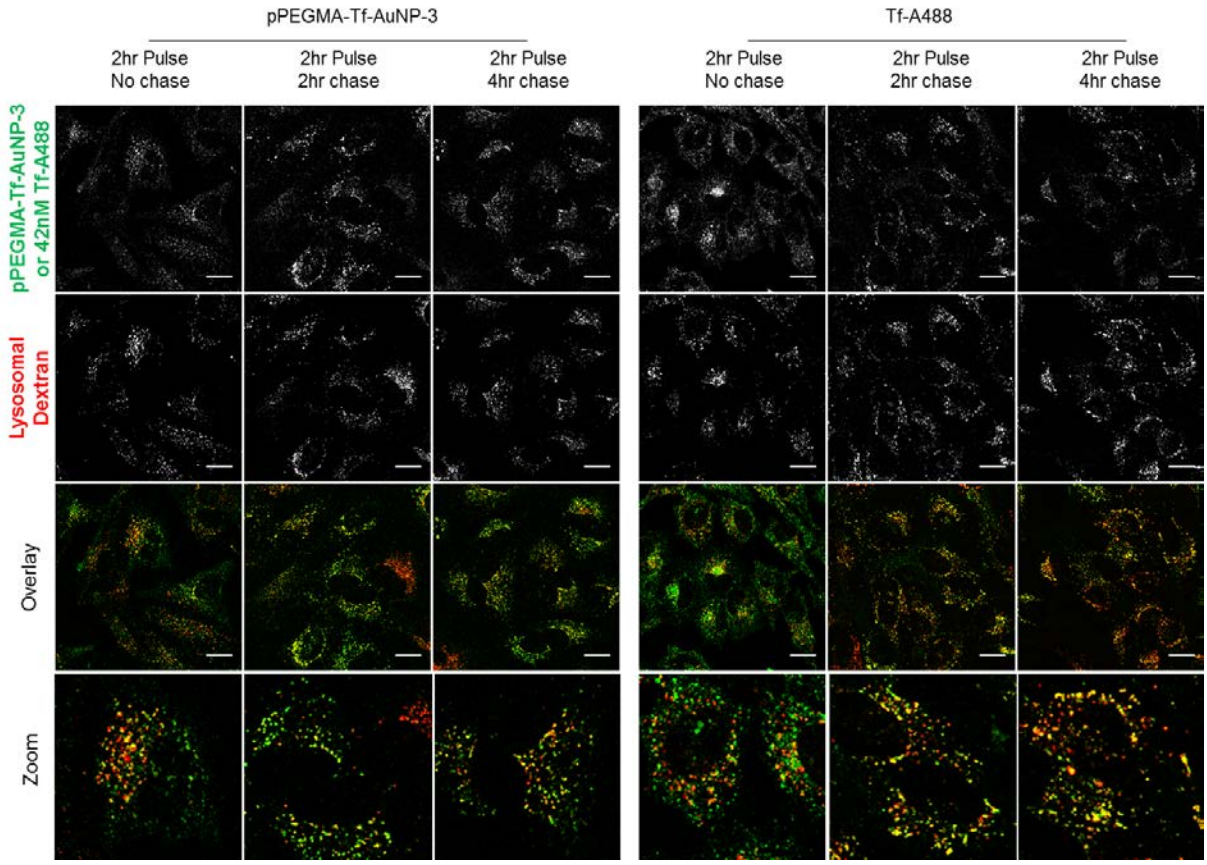

Figure 6: Uptake of pPEGMA-Tf-AuNP-3 or equivalent Tf and their lysosomal localization over time. Lysosomes were pre-loaded with Dextran-A647 (red) by incubating cells with 100 μg/mL Dex647 for 2 h, washed and chased overnight. pPEGAM-Tf-AuNP-3 or 42 nM Tf-A488 were incubated with the cells for 2 h in serum free medium containing BSA, washed with imaging medium containing 10% FBS, imaged immediately and again at 2 h and 4 h post washing. Images represent single section confocal images, scale bars = 20 μm, and the 'zoomed' micrographs are all contrast enhanced by the same amount to increase clarity in printed images.

Uptake of the nanoparticles was again low, but nevertheless, the pPEGMA-Tf-AuNP-3 signals were apparent in lysosomal compartments at the early time periods. However, the signal from Tf was also visible after 6 hours, i.e. considerably in excess of the normal residence time of transferrin in normal cell culture. Accordingly, this suggested that at 41 °C and the concentrations of Tf used in the assay (42 nM, calculated to be equivalent to those of Tf on the

pPEGMA-Tf-AuNP-3 particles), the internalization of Tf occurred via more than one pathway, i.e. fluid-phase endocytosis as well as the normal receptor-mediated endocytic pathway. However, there was a notable drop in intensity of Tf-A488 following the first 2 h chase indicating that some Tf was recycled as expected, but no similar drop in intensity was apparent in the fluorescence from pPEGMA-Tf-AuNP-3 suggesting little evidence of recycling.

DISCUSSION

Functionalisation of nanoparticles with responsive polymer transferrin conjugates

Transferrin (Tf) has been widely used as a targeting agent for drug delivery and many examples exist in the literature reporting the success of Tf-conjugated materials *in vitro*[28, 36-38] and, to a lesser extent, *in vivo*.[25, 27, 39] In parallel, there has been a number of articles describing how responsive polymers have been utilized to control accessibility of small molecule targeting ligands through conformational changes.[40-42] The combination therefore of responsive polymers with Tf functionality seemed an appealing option for controlling cell entry of nanoparticles, but at the start of the study there were no reports of macromolecular ligands such as Tf being 'hidden and revealed' via an external stimulus. In addition, the display of any targeting ligand and its presentation to cell-surface receptors is crucial to its activity. The Dawson group has pioneered the study of adsorbed protein layers on nanoparticle delivery,[43-45] and showed conclusively that Tf-functionalized nanoparticles can lose targeting specificity as a consequence of becoming inaccessible due to protein coating in sera.[14] We therefore based our design principles around nanoparticles with an inner shell formed of a poly(zwitterion), poly(2-methacryloyloxyethyl phosphorylcholine (pMPC), which has been reported to confer resistance to protein opsonization,[46-48] onto which Tf could be conjugated. As with previous studies, we utilized a short oligoethyleneglycol spacer between the Tf and the polymer chain, and adopted cyclooctyne click chemistry to connect the protein and spacer to azido-functional

side-chains co-polymerized into the pMPC inner shell. We thus expected Tf to retain accessibility in the cellular environment in the absence of any further derivatization with an outer responsive polymer layer in a hydrophilic 'stealth' conformation. In this way, an average of 1, 2 and 3 Tf molecules was appended to each of the pMPC-derivatized gold nanoparticles (denoted as Tf-AuNP-1, 2 and 3 respectively). The responsive polymer outer layer was also attached via click chemistry routes, using a cyclooctyne-terminated pPEGMA with a cloud point of 39 °C. The presence of Tf likely provided hindrance to the attachment of the pPEGMA chains, as while ~ 7 polymer chains were attached to nanoparticles with one appended Tf, ~ 4 pPEGMA chains were conjugated to Tf-AuNP-2 and only 2 pPEGMA chains were linked to Tf-AuNP-3. This was perhaps not unexpected, as the AuNPs were of 15 nm diameter, the pMPC layer was expected to be ~ 5 nm thick based on molar mass and polymer chain length calculations, and Tf spans nearly 8 nm in one dimension. The pendant proteins would thus have provided a considerable barrier to a 'brush' polymer such as the pPEGMA materials synthesized for this study, which were themselves likely to have been at least 7 nm in length based on calculated end-to-end distances.

SPR data showed that the pMPC-AuNPs were the least bound of all the NPs at the Tf-receptor (TfR) functionalized SPR substrates, confirming the resistance of the primary zwitterionic layer to non-specific adsorption at surfaces when in buffered aqueous media. These experiments also demonstrated that the pPEGMA-Tf-AuNPs attached to the greatest extent, indicative of a synergistic effect of the thermoresponsive polymer outer layer on surface attachment in addition to the expected Tf-TfR bio-recognition interactions. In all cases except for the pMPC-AuNPs, attachment to the SPR sensor chip surface increased with temperature, again suggestive that the associations with the SPR substrates were not solely a function of Tf-TfR binding.

Nanoparticle internalization in cancer cells

Investigations of nanoparticle endocytosis were conducted in HeLa cells in accord with previous protocols.[41, 42] Conditions of low particle concentration were chosen to minimize self-association of nanoparticles at temperatures above which the pPEGMA chains were expected to undergo coil-to-globule transitions, as this has been a confounding factor in prior responsive particle endocytosis experiments,[49, 50] but this constraint meant that the assays were close to the limits of accurate quantitation of nanoparticle uptake. We also worked in low protein media (DMEM + 0.1 % BSA) to reduce the potential for protein corona formation. As apparent from Figure 3, the highest internalization was shown by pPEGMA-Tf-AuNP-3 at a temperature (41 °C) above the PAT of the polymer, with very low uptake of the other NPs at temperatures above or below the PAT. While on first inspection this result might be attributed to the intended 'switch' of accessibility of Tf as the polymer chains in pPEGMA-Tf-AuNP-3 collapsed, thus revealing the ligand to cell surface receptors, there are other factors which likely affected internalization. The pPEGMA-Tf-AuNP-3 particles were the least negatively charged of all the NPs in the sample set, and thus were least likely to have invoked charge-charge repulsion at HeLa cell surfaces. Similar particle charge effects would not have been as significant in the SPR experiments, as the substrates in those assays are dextran-based and thus rather different in charge and chemical composition to cell surfaces. Thus it may have been possible that the differences in binding behavior of the NPs in the variable-temperature endocytosis study compared to those in the SPR assays were a combined function of charge, accessibility of Tf and hydrophilicity/hydrophobicity of the pPEGMA outer layer around its aggregation temperature. In addition, although there were no proteins in the SPR assay media other than Tf, there were proteins (albeit at low concentrations) in the cell culture media used for the nanoparticle uptake experiments in HeLa cells. It is therefore possible that adsorption of these media proteins to nanoparticles may nevertheless have taken place, and in such a case, the

exposed Tf proteins on nanoparticles with no outer pPEGMA layer may have been passivated by serum proteins in a manner analogous to that reported by Salvati *et al.*[14]

Intracellular trafficking of responsive polymer transferrin conjugate nanoparticles

The intracellular locations of the internalized nanoparticles were evaluated on the basis that a specific transferrin-receptor (TfR) mediated pathway would lead to routing of the nanoparticles and entry into a recycling pathway, as has been well characterized for transferrin. Again, we kept concentrations low to avoid any self-association of nanoparticles, but the experiments showed that while uptake of pPEGMA-Tf-AuNP-3 was highest as expected based on the previous data, all the nanoparticles were observed in lysosomal compartments (Figure 4). This suggested that the Tf-functionalized nanoparticles entered the cells also via some non-specific uptake routes (i.e, not mediated by Tf), or were re-routed to lysosomes following internalization rather than following the conventional Tf recycling pathway, again in accord with some of the findings of Salvati *et al.*[14]

Through further investigation we showed a dependence on TfR for the uptake of pPEGMA-Tf-AuNP-3 particles (Figure 5). This suggested that the majority of these specific particles were internalizing through a TfR dependent pathway and being re-routed to the lysosome rather than through a non-selective uptake pathway. We have previously shown that binding (crosslinking) multiple TfR using biotinylated antibody crosslinked with streptavidin, were re-routed to the lysosome rather than being recycled. We therefore speculate that the presence of more than one Tf protein on each pPEGMA-Tf-AuNP-3 had the ability to cross-link the TfR as a result of a multivalent effect and hence drive the particles to the lysosome. However, it has been noted before that absolute cell uptake of nanoparticles is not necessarily correlated with specific receptor-mediated endocytic processes, as generalized pinocytic routes can lead to particle internalization in addition to those via selective ligand-receptor interactions.[44]

An additional complexity in the nanoparticle uptake experiments was the potential for changes in both receptor-mediated and generalized pinocytic internalization pathways with temperature. We therefore carried out pulse-chase experiments with both Tf-488 and the pPEGMA-Tf-AuNP-3 nanoparticles (Figure 6). As apparent from the confocal micrographs in Figure 6, there was little change in the fluorescence intensities arising from the pPEGMA-AuNP-3 in the cells at 2, 4 and 6 hrs and colocalization with the lysosomes was evident from the start. This indicated that pPEGMA-Tf-AuNP-3 internalized rapidly and trafficked to the lysosome with no recycling. Fluorescence from Tf-488 was apparent after 2hrs with the majority not localized to lysosomes, however, after 4 and 6hrs, well-beyond the normal time for Tf-recycling, Tf-488 was observed colocalizing with the lysosomal marker although overall Tf intensity was lower. These data indicated that a population of Tf was being internalized through fluid phase routes and localizing to the lysosome while the remainder was still recycling out of the cell.

The difference in behavior between Tf-488 and pPEGMA-Tf-AuNP-3 suggest there are differences in their endocytosis once within the cell. While uptake of pPEGMA-Tf-AuNP-3 was shown to be through the TfR, these nanoparticles quickly localized to the lysosome and showed no evidence of recycling in contrast to Tf-488. We suspect that in our assays Tf-488 remained fully bioavailable, thus binding TfR and saturating the receptor (typical K_D = 1-10nM), leading to internalization through alternative, non-specific pathways. However, when Tf was attached to pPEGMA-Tf-AuNP-3, its mode of binding to TfR may have prevented saturation of the receptor to the same extent as for the rather smaller Tf-488. This in turn may have routed pPEGMA-Tf-AuNP-3 to the lysosome, possibly through a receptor crosslinking-dependent pathway, while the portion of ‘free’ Tf-488 which localized to the lysosome was likely to have been Tf-488 which was internalized through non-specific pathways.

When considered overall, the results in this study show that while the tailoring of surface coating with functional components and targeting agents can be used to control the delivery of nanoparticles to cells, there are nevertheless clear confirmations of the inherent complexity of cell entry mechanisms for nanoparticles. Our data for lysosomal accumulation of Tf-bearing nanoparticles were as noted above in accord with those of Salvati *et al* who observed similar trafficking for Tf-PEG-silica nanoparticles,[14] but different to those of Choe *et al* who reported recycling of Tf-tagged polypeptide vesicles.[38] Our results showed that the pPEGMA-Tf-AuNP-3 particles were the most internalized of all those tested at 41 °C, i.e. when the outermost polymer chains on their surface were expected to be collapsed and Tf exposed to interact with cell surface receptors. However, our data also indicated that particles may internalize by non-Tf pathways too, and thus it is likely that a combination of ligand accessibility, surface hydrophobicity and surface charge were all contributors to the endocytic mechanisms and the enhanced accumulation of pPEGMA-Tf-AuNP-3 compared to the other nanoparticles.

It should also be noted that extension of these studies to an *in vivo* setting would require verification first that the nanoparticles retain accessibility of the Tf ligand in the circulatory system or in any extracellular matrix in which these materials might be injected.[14] There is also the caveat that the outer responsive layer becomes more protein adsorbent when it is chain-collapsed. Thus, under conditions of local hyperthermia *in vivo*, which can occur via external stimulus or local disease in tissues such as solid tumors, the exposure time for the nanoparticles prior to encounter with cell surface transferrin receptors might be critical for in determining whether the outer layer adsorbs a 'blocking' corona of extracellular matrix biopolymers.[13, 51] Nevertheless, the initial indication that nanoparticle endocytosis can be switched by hiding/revealing a protein ligand in cell culture conditions is promising, and suggests that if a polymer conformational and steric barrier change could be triggered without invoking a

concomitant alteration in nanoparticle surface hydrophobicity, a powerful means to target specific cells or tissues via external stimulus could result.

Experimental Section

Materials

Thio-transferrin[52] was kindly donated by Albumedix Ltd, Nottingham, UK and used as received. PD SpinTrap G-25 columns, Disposable PD-10 Desalting Columns, Vivaspin 6 (MWCO 100K), Hiprep 26/60 columns, Biacore NTA sensor chip, NTA reagent kit and HBS-P buffer were purchased from GE Healthcare Life Sciences. Alexa Fluor 488-SDP and Dulbecco's Modified Eagle Medium (DMEM) without phenol red was purchased from Thermo Fisher Scientific. Hydrogen tetrachloroaurate hydrate (99.999% trace metal basis) was purchased from Acros Organics. All solvents and reagents were of analytical or HPLC grade and purchased from Sigma Aldrich unless otherwise specified. Tri(ethylene glycol)ethyl ether methacrylate (TriEGMA, M_n 246 g mol^{-1}) and polyethylene methyl ether methacrylate (pPEGMA, M_n 475 g mol^{-1}) were purchased from Sigma-Aldrich and purified by passing through a column filled with basic alumina before use. Holo-Transferrin Human (≥ 98%), 2-Methacryloyloxyethyl phosphorylcholine (MPC, 97%), 2-[2-(2-Chloroethoxy)ethoxy]ethanol (96%), Sodium azide (≥ 99.5%), Potassium iodide (≥ 99%), Triethylamine (Et3N (≥99%)), Methacryloyl chloride (97%), (±)-α-Lipoic acid (98%), 2-Hydroxyethyl disulfide (90%), *N,N′*-Diisopropylcarbodiimide (DIC, ≥98%), 4-(Dimethylamino)pyridine (DMAP, ≥98%), α-Bromoisobutyryl bromide (98%), 2,2'-bipyridyl (≥98%), Dibenzocyclooctyne-PEG4-maleimide, 5,5′-Dithiobis(2-nitrobenzoic acid) (≥98%), Copper (II) Bromide (Cu(II)Br_2, 99%), Copper (I) Bromide (Cu(I)Br, >98%), Ethylenediaminetetraacetic acid disodium salt (EDTA, >99%), Fetal Calf Serum (FCS) and PBS Dulbecco (Modified, without calcium chloride and magnesium chloride) were purchased from Sigma Aldrich.

NMR analysis

^{1}H NMR spectra were recorded on a Bruker 400 spectrometer at 399.8 MHz (^{1}H) and 100.5 MHz (^{13}C) with samples prepared in in $CDCl_3$ or D_2O. All chemical shifts are reported in ppm relative to TMS.

Gel Permeation Chromatography (GPC) analysis

Organic solvent conditions:

Gel Permeation Chromatography (GPC) was performed on a Polymer Labs GPC 50 Plus system fitted with a differential refractive index detector. Separations were performed on a pair of PLgel Mixed-D columns (300 7.8 mm, 5 mm bead size, Polymer Labs UK) fitted with a matching guard column (50 7.8 mm). Chromatograms were run at 40 °C using chloroform ($CHCl_3$) as eluent with a flow rate of 1 ml/min. Column calibration was achieved using narrow polystyrene standards (160 Da–240 kDa, Agilent, UK).

Aqueous solvent conditions:

Aqueous GPC was performed on a Shimadzu Prominence UPLC system fitted with a DGU-20A5 degasser, LC-20AD, CBM-20A LITE system controller, SIL-20A autosampler, CTO-20A oven and RID-10A refractive index detector. Separations were performed on a series of Aquagel 30-40-50 (300 x 7.8 mm, 5 mm bead size, Agilent UK) columns fitted with a matching guard column (50 x 7.8 mm). Analysis was carried out at 35°C. The mobile phase was Dulbecco PBS buffer pH 7.4 at a flow rate of 1 mL/min. Column calibration was achieved using Polyethylene oxide/glycol EasiVials (2 mL) standards (196 Da–498 kDa, Agilent UK).

Protein and polymer bioconjugate analysis

Aqueous GPC for bioconjugates was performed on a Shimadzu Prominence UPLC system as above. Protein conjugate: GPC analysis was performed in isotonic PBS pH 7.4 (Dulbecco) using a TSKgel G3000SWXL, TOSOH column, UV absorbance was recorded at 220/280 nm.

Thermoresponsive polymers: GPC analysis for responsive polymer-protein conjugates was performed in isotonic PBS pH 7.4 (Dulbecco, DPBS) with 10% methanol using a Aquagel 30 column (Polymer Labs), UV absorbance was recorded at 220 nm.

UV-Vis analysis

UV-Vis spectra for AuNPs solutions were recorded on a Cary UV/Vis spectrometer over the range 200-800 nm.

Cloud point analysis of polymers/AuNP protein polymer conjugates and colloidal stability analysis of AuNP in media were carried out using a Beckman DU 800 UV/Vis Spectrophotometer with a Peltier Temperature Controller.

Cloud point measurements

UV absorbance was recorded at 550 nm (or 534 nm). The samples solutions were heated from 20°C to 65°C using a temperature gradient of 0.5°C/min and UV readings were recorded every 0.5°C.

Centrifugal purification

High speed centrifuge - Particles were separated by centrifugation using a Beckman J2 centrifuge with JA-17 fixed angle rotor. Particles were centrifuged at 4°C and 21 kG for 45 minutes. The supernatant was recovered, the particle resuspended in isotonic PBS and the process repeated as required.

Low speed centrifuge (bench centrifuge) – Particles were concentrated at room temperature using a Technico Maxi bench centrifuge. The solutions were transferred to 1.5 mL Eppendorfs and centrifuged at 16kG for 45 minutes. The particles were resuspended in a small amount of isotonic PBS, sterile filtered (0.22 μm PES) and kept in fridge until further analysis.

Zeta potential measurements

Zeta potential measurements and hydrodynamic radii of the AuNP-protein polymer conjugates were measured using a Malvern Zetasizer Nano ZS. Dynamic light scattering (DLS) at 173° angle and z-potential measurements were performed at 33°C, 37°C and 41°C. Samples were allowed to equilibrate for 8 minutes at each new temperature before acquisition. All samples were prepared in 1/100 DPBS buffer. Data analysis was carried out using Zetasizer Software (version 7.11).

Dynamic light scattering (DLS)

Dynamic light-scattering was performed using a Viscotek 802 DLS instrument fitted with an internal laser (λ 830nm ± 5 nm, P_{max} 60 mW). Laser power was adjusted until a detection rate of at least 300 kcps was achieved. The samples were measured across a temperature range of 25-41°C. Experimental scattering data were recorded for three seconds for each sample and repeated ten times for each temperature point. Hydrodynamic radii distributions were calculated with Viscotek/Malvern OmniSize3 software.

Size exclusion purification

Protein and gold colloid purifications were carried out using a Hi-Prep 26/60 (Sephacryl S-200) column. Separations were carried out in isotonic PBS on Agilent 971-FP system using UV detection at 220/280 nm and a flowrate of 2.0 mL/min.

SPR analysis

Surface plasma resonance (SPR) analysis was carried out on a Biacore 3000 instrument using a NTA chip. The NTA chip was activated according to manufacturer's specification. TfR-His tag was used to conjugate to the Ni decorated surface, RU= 800 (reference channel was left unmodified). HBS-P buffer supplemented with 200 mM NaCl was used as the running buffer at a flowrate of 50 µL/min. A 120 second injection time was used for each injection, followed by 6 minutes dissociation. The surfaces were regenerated by washing with 3M NaCl for 4 minutes and then allowing to equilibrate for 15 minutes before subsequent injections. AuNP stocks were diluted by a factor of 16 to 50 depending on AuNP initial concentration in order to normalize concentrations. Binding experiments were carried out at 25°C and 37°C respectively.

TEM analysis

Transmission Electron Microscopy (TEM) analysis was performed on a FEI Tecnai 12 Biotwin transmission electron microscope. Solutions of AuNP aqueous samples (10 µL) were placed on a TEM copper grid coated with formvar carbon film for a few minutes. The excess solution was subsequently removed with filter paper and the grid dried over 2-3 hours before TEM imaging.

Colloidal stability

The AuNP solutions were diluted with DMEM by a factor of 15.5 to 31 depending on AuNP initial concentration in order to normalize concentrations. The solutions were placed in a spectrophotometer at 37 °C and the absorbance monitored at λ = 534 nm (AuNP maximum) over a period of 240 minutes. A reading for each sample was taken every 20 seconds. Absorbance readings were normalized for each AuNP batch to 100% at t= 0 minutes.

Synthesis of 14-bromo-14-methyl-13-oxo-3,6,9,12-tetraoxapentadecyl 5-(1,2-dithiolan-3-yl)pentanoate (Lipoic acid–TEG-ATRP initiator) (Compound **1**, Figure 1)

Precursor compound 2-(2-(2-(2-hydroxyethoxy)ethoxy)ethoxy)ethyl 2-bromo-2-methylpropanoate (HO-TEG-Br) was synthesized and analyzed as reported previously.[53]

(±)-α-Lipoic acid (0.75 g, 3.6 mmol) and HO-TEG-Br (1.2 g, 3.5 mmol) were weighed out and placed in a round bottom flask. The compounds were dissolved in anhydrous dichloromethane (50 mL) and the solution cooled down to 0 °C in an ice bath. Diisopropylcarbodiimide (DIC, 0.92 g, 7.3 mmol) and DMAP (catalytic amount) were added to the solution. The solution was allowed to heat up to room temperature and then left to react overnight. The following day the solution was filtered and the precipitate discarded. The solvent was removed under reduced pressure and the product purified by silica column chromatography using a 20% *n*-hexane/80% Et_2O → 100% Et_2O solvent mixture. The Lipoic –TEG-ATRP initiator was collected as yellowish oil (1.3g, 70% yield). ^{1}H NMR ($CDCl_3$, 400 MHz): δ 4.34-4.32 (t, 2H), 4.24-4.2 (t, 2H), 3.76-3.73 (t, 2H), 3.72-3.62 (m, 10H), 3.60-3.53 (m, 1H), 3.22-3.08 (m, 2H), 2.50-2.42 (m, 1H), 2.38-2.33 (m, 2H), 1.94 (s, 6H), 1.94-1.87 (m,1H), 1.74-1.64 (m,4H), 1.55-1.38 (m,2H). ^{13}C NMR ($CDCl_3$, 100 MHz): δ 173.44, 171.62, 70.75, 70.67, 70.65, 70.59, 69.19, 68.77, 65.13, 63.46, 56.34, 55.72, 40.22, 38.49, 34.60, 33.95, 30.77, 28.74, 24.62.

Synthesis of 2-(2-(2-azidoethoxy)ethoxy)ethyl methacrylate (Azido-TriEG-Methacrylate) (Compound **2** Figure 1).

2-(2-(2-Chloroethoxy)ethoxy)ethanol (20 g, 0.12 mol), sodium azide (15.4 g, 0.227 mol) and potassium iodide (~ 0.5 mol % added as catalyst) were placed in a round bottom flask and dissolved in 100 mL of water. The mixture was heated under reflux at 100 °C for 3 days. The solution was then cooled down and the product extracted with ethyl acetate (3 x 100 mL). The organic layer was dried with sodium sulfate and then removed under reduced pressure. Azido-TriEG was recovered as yellowish oil (18g, 86% yield). ^{1}H NMR (Acetone-d6, 400 MHz): δ 3.71-3.69 (t, 2H), 3.68-3.60 (m, 6H), 3.56-3.53 (t, 2H), 3.42-3.39 (t, 2H).^{13}C NMR (Acetone-d6, 100 MHz): δ 72.67, 70.3 (multiple signals), 69.8, 61.1, 50.50.

Azido-TriEG (3.0 g, 0.017 mol) was placed in a sealed round bottom flask and dissolved in anhydrous DCM (50 mL). The solution was cooled down to 0°C in an ice bath and triethylamine (2.6 g, 0.025 mol) was added. Methacryloyl chloride (1.8 g, 0.017 mol) was subsequently added dropwise to the reaction, and allowed to react overnight. The solution was then filtered, and the precipitate discarded. The solvent was removed under reduced pressure and the product purified by silica chromatography (mobile phase: 66 % n-hexane/33% ethyl acetate vol:vol). Azido-TriEG-Methacrylate was recovered as yellowish oil (3.5 g, 85% yield).

^{1}H NMR ($CDCl_3$, 400 MHz): δ 6.14-6.13 (m, 1H), 5.58 (m, 1H), 4.32-4.30 (t, 2H), 3.77-3.75 (t, 2H), 3.70-3.66 (m, 6H), 3.40-3.38(m, 2H), 1.96-1.95(s, 3H). ^{13}C NMR ($CDCl_3$, 100 MHz): δ 167.35, 136.17, 125.71, 70.72-69.25 (multiple signals), 63.85, 50.70, 18.31.

Synthesis of disulfanediylbis(ethane-2,1-diyl) bis(2-bromo-2-methylpropanoate) (Disulfide ATRP initiator) (Compound **3** in Figure 1).

2-Hydroxyethyl disulfide (11 g, 0.071 mol) was placed in a round bottom flask and dissolved in anhydrous DCM (100 mL). The solution was cooled down to 0°C in an ice bath and

triethylamine (14.9 g, 0.146 mol) was added. Bromoisobutyryl bromide (32 g, 0.14 mol) was added dropwise to the reaction and allowed to react overnight. The solution was then filtered and the precipitate discarded. The solvent was removed under reduced pressure and the product purified with silica chromatography (mobile phase: 50 % *n*-hexane/50% Et_2O). The product was recovered as a yellow oil (25 g, 77% yield).

^{1}H NMR ($CDCl_3$, 400 MHz): δ 4.46-4.43 (t, 4H), 3.00-2.97 (t, 4H), 1.95-1.94 (s, 12H) ^{13}C NMR ($CDCl_3$, 100 MHz): δ 171.43, 63.52, 55.51, 36.78, 30.73.

Preparation of end- and side-chain reactive poly(2-methacryloyloxyethyl phosphorylcholine)s (Corona polymer CP-1)

Lipoic–TEG-ATRP initiator (**1**, Figure 1; 30 mg, 0.05 mmol) was dissolved in 4.3 mL of deoxygenated methanol and transferred into a sealed round bottom flask. Cu(I)Br (8 mg, 0.05 mmol) and 2,2' bipyridyl (18 mg, 11 mmol) were added to the flask and allowed to dissolve completely. The polymerization was initiated by the addition of the MPC monomer (1.67 g, 5.64 mmol). Conversion of the polymerization was monitored using ^{1}H-NMR. When the conversion of monomer had reached 82% (150 minutes), a deoxygenated solution of MPC monomer (167 mg, 0.56 mmol) and Azido-TriEG-Methacrylate (compound **2**, Figure 1, 35 mg, 0.28 mmol) was added using a cannula. The polymerization was stopped after 210 minutes by exposing the solution to air. Total conversion after 210 minutes was 85% by ^{1}H-NMR. Copper, bipyridyl and monomer were removed by dialysis (MWCO 6-8000) in water in the presence of EDTA. The dialysis bag was placed into pure water before lyophilisation and collection of the polymer. A white crystalline powder (1.0 g) was collected after lyophilisation (lipoate-terminated and azide-functional polyMPC, corona polymer CP-1). Monomer conversion was calculated from ^{1}H-NMR spectra by comparing the vinyl proton signals from the monomers (5.6 and 6.1 *ppm*) to the integration of 6 MPC protons from 4.3 to 3.9 ppm.

The monomer composition of CP-1 was calculated by comparing the ratio of the methyl (-CH_3, 9H) signals for MPC at 3.18 ppm to the CH_2 signals from MPC (2H) and Azido-TriEG (8H) at 3.6 ppm. For every unit of MPC in the final polymer there were 0.028 units of Azido-TriEG present. The degree of polymerization was ~110, indicating ~ 3 units of Azido-TriEG were present in the final polymer.

Molar masses and mass distributions of polymers were determined using aqueous gel permeation chromatography (DPBS, Aquagels 30-40-50).

pPEGMA polymerization

Disulfide ATRP initiator (compound 3, Figure 1, 50 mg, 0.11 mmol), DiEGMA (3.6 g, 19 mmol), PEGMA475 (1.5g, 3.1 mmol) and 2,2'-bipyridyl (69 mg, 0.44 mmol) were placed in a round bottom flask, dissolved in 15 mL of toluene and the flask sealed. The solution was deoxygenated by bubbling argon through it for 30 minutes. The reaction heated to 70°C and Cu(I)Cl (22 mg, 0.22 mmol) was added to the flask to start the polymerization. The polymerization was allowed to progress overnight. The following morning the polymerization was stopped by exposing the reaction to oxygen and cooling it down. Monomer conversion was calculated from ^{1}H-NMR spectra by comparing two the vinyl proton signals from the DiEGMA and PEGMA475 monomers (5.6 and 6.2 ppm) to the integration of protons from 4.4 to 4.0 ppm. In the region of 4.0-4.4 ppm two protons from the polymer resonate plus two protons from the monomers. Conversion was calculated by subtracting the monomer signal in the region 4.0-4.4 ppm from the total integration and dividing it with the total integration signal. The conversion of the polymerization was 95% by ^{1}H-NMR. Degree of polymerization was therefore 95 units per polymer chain according to ^{1}H-NMR analysis. The polymer was purified by passing the polymer solution through a short column of alumina and precipitation into a mixture of hexane/ether (75/25). The precipitate was dissolved in DCM and the polymer

precipitated again in a hexane/ether mixture, this process was repeated twice. The pPEGMA disulfide polymer (1.7 g) was recovered as a yellowish sticky oil.

The composition of PEGMA475 and DiEGMA in the polymer was calculated from the NMR spectra of the purified polymer in $CDCl_3$. The ratio of PEGMA 475 to DiEGMA in the polymer was determined by comparing the integral of the methoxy (-OMe) protons (3.45-3.35 ppm) to the ethylene glycol polymer backbone (3.85- 3.55 ppm). In the ethylene glycol polymer region the PEGMA475 has 34 protons while DiEGMA has 6 protons relative to the methoxy protons (-OMe). The purified polymer had 9.54 protons in the ethylene glycol region. The molecular composition of the purified polymer was thus 12.6% PEGMA475 and 87.4% DiEGMA, i.e. 34xPEGMA475 + 6xDiEGMA = 9.54 (DiEGMA+PEGMA475= 1).

Molar masses and mass distributions of polymers were determined using organic gel permeation chromatography (Chloroform, PLgel Mixed-D Columns).

Synthesis of thermoresponsive polymer TRP-1 by pPEGMA-disulfide polymer reduction and DBCO functionalisation

Reduction of pPEGMA-disulfide: A sample of pPEGMA-disulfide (264 mg, 6.3 µmol) was dissolved in 1 mL isotonic PBS (pH 7.4). To this, an aliquot (0.4 mL) of 0.5 M EDTA solution (pH 8.0) was added, to give a 50 mM final EDTA concentration. Then, a sample (0.32 mL) of a 25 mg/mL TCEP solution (18 mg, 63 µmol) was added to the polymer solution and the reaction was continued overnight at 4 °C. The following morning the solution was passed through a PD10 desalting column (eluent PBS and 5 mM EDTA) to remove the free TCEP from the solution. The cleaved polymer was characterized in terms of molar mass by GPC ($CHCl_3$) and for thiol content by Ellman assays. The polymer solution, denoted as pPEGMA-SH was kept at 4 °C prior to maleimide conjugation.

DBCO functionalization: pPEGMA-SH (82 mg, 3.3 µmol) in 2.25 mL of isotonic PBS pH 7.4 containing 5 mM EDTA was mixed with dibenzocyclooctyne-PEG4-maleimide linker (16.2 mg, 24 µmol (DMSO stock 50 mg/mL)) and allowed to react overnight at 4 °C. The solution was then passed through a PD10 desalting column using a DPBS eluent to remove the free DBCO linker from the reaction. The extent of modification was verified via Ellman assays and the resultant conjugate polymer checked by GPC to ensure no oxidation had occurred during the conjugation. Polymer solutions were stored at 4 °C.

Gold nanoparticle (AuNP) synthesis

A solution of $HAuClO_4$ (393 mL, 1.0 mM) was placed in a 500 mL round bottom flask and heated up to 100 °C. A solution of aqueous sodium citrate tribasic (137.5 mL, 38.8 mM) at ~ 100 °C was added to the gold solution, gently agitated and allowed to react for 10 minutes. After 10 minutes the solution was cooled down to room temperature and then stored at 4 °C until required.

Particles were analyzed by UV-Vis, and disc centrifuge (CPS). Calculations of nanoparticle numbers used in experimental assays were based on measurements of particle size (CPS), the density of gold and dilutions of stock solutions of known concentration.

AuNP functionalization with polymer CP-1

A solution of AuNPs (400 mL, 1.71 x 10^{15} particles total, 2.84 nmol) was measured into polypropylene (PP) containers. Corona polymer CP-1 (355 mg, 14,200 nmol, 5000 eq,) was dissolved in 4 mL of water and distributed equally among the AuNP-containing containers. The containers were placed on rollers at room temperature and allowed to react overnight. The AuNP solutions were transferred into 50 mL PP centrifugal tubes and centrifuged (21kG at 4°C) for 45 minutes, the supernatant was removed and kept for analysis. The polymer

concentration in the initial supernatant was estimated using Aqueous GPC (TSKgel) and compared to that of the initial polymer stock in order to estimate polymer grafting onto the AuNPs. The pellets were then resuspended in isotonic PBS, centrifuged again at 21kG for further 45 minutes and the supernatant discarded. This process was repeated once. The pellets were subsequently dissolved in a minimal amount of PBS and transferred into Eppendorf tubes. The solutions were centrifuged at 16kG for 45 minutes and the supernatant discarded. The pellets were redissolved in PBS and the process repeated once. Finally all the pellets were redissolved in PBS and all the aliquots pooled together (12.8 mL total volume). The polymer-AuNP (AuNP-CP-1) solutions were filtered through 0.22 µm PES membrane. Small portions of the purified AuNP-CP-1 solutions were centrifuged and analyzed for free polymer by GPC in order to ensure the purification was complete. The particle concentration was measured by spectroscopy and compared to particle concentration of the stock AuNP solution to determine the recovery yield. Particle recovery was almost quantitative and aqueous GPC of the supernatant revealed that 10% of the polymer had conjugated to the AuNP, i.e. ~ 500 polymer chains were grafted onto each AuNP. The concentration of the purified AuNP-CP-1 solution was 1.34 $x10^{14}$ NP/mL.

Thio-transferrin- Dibenzocyclooctyne/Alexa Fluor 488 functionalisation

An aliquot (7 mL) of a 5 mg/mL thiotransferrin solution (Tf content, 35 mg, 0.4 µmoles) in 10 mM HEPES pH 7.4 was taken from -80°C freezer, gently thawed and allowed to reach room temperature. Dibenzocyclooctyne-PEG4-maleimide (DBCO) linker was dissolved in DMSO in order to make a 50 mg/mL stock solution. A sample from this stock solution (8 µL= 0.41 mg, 0.6 µmol DBCO) was added to protein solution and allowed to react for 3 hours at room temperature. The mixture was subsequently purified using a HiPREP 26/60 column to remove any thio-Tf protein dimers and unreacted DBCO linker. Purity was determined by GPC

(TSKgel, DPBS) analysis and compared to the starting thioTf**.** The concentration of the purified TF-DBCO and subsequent yield of recovery was determined by UV spectroscopy at λ = 280 nm. Recovery of thioTf after HiPrep purification was 17 mg (49% protein recovery). GPC analysis of the purified conjugate revealed that the Tf-DBCO was 70% pure, with approx. 30% unconjugated Tf species. The Tf-DBCO conjugate was stored at 4 °C.

Tf-DBCO Alexa Fluor 488 SDP conjugation:

The reactive dye Alexa Fluor 488 SDP (AF488 SDP) (1 mg) was dissolved in 0.1 mL of anhydrous DMSO to form a 10 mg/mL stock. An aliquot of1.0 mL of Tf-DBCO (14.3 mg, 0.178 µmol) in isotonic PBS pH 7.4 was mixed with 0.2 mL of 1 M Sodium bicarbonate buffer pH 8.3. An aliquot (73 µL) of AF488 SDP stock solution (AF488SDP content = 0.737 mg, 0.893 µmol, 5 molar eq. to Tf) was added to the protein solution while the solution was gently stirred. The solution was reacted overnight at 4 °C. The unreacted dye was removed using a PD10 column (gravity protocol) and isotonic PBS as eluent. The Tf-DBCO-AF488 conjugate was recovered after PD10 purification. The protein concentration/dye ratio was determined by UV-vis absorbance at λ = 280/494 nm and calculated according to the manufacturer's (Invitrogen) specifications.[33] A total of 13.6 mg of Tf-DBCO-AF488 (30% TF-AF488) was recovered after gel permeation chromatography purification, and the level of Alexa Fluor 488 labelling was 2.7 dye molecules per protein. The Tf-DBCO-AF488 was aliquoted into Eppendorf tubes, frozen with liquid nitrogen and stored at -80°C.

Tf-DBCO - Particle conjugation

AuNP-CP-1 stock solution was transferred into 15 mL falcon tubes and diluted by a factor of two using isotonic PBS. Tf-DBCO-AF488 (3.9 mg/mL stock ~ 70% pure) was added to the falcon tubes in appropriate amount to give a particle ratio of two, four and eight Tf per AuNP.

The AuNP-Tf solutions were allowed to react at 4°C for 3 days at low speed on an orbital shaker. After 3 days the solutions were diluted down to a total volume of 15 mL using isotonic PBS. The particles were transferred to 50 mL centrifuge tubes and centrifuged at 21kG for 45 minutes at 4°C. The supernatant was collected and AF488 fluorescence quantified by spectrofluorometry. Protein grafting density was determined by comparing the AF488 fluorescence in the supernatant to that of the protein AF488 stock. The pellets were then resuspended in PBS (50 mL each), the solutions centrifuged again at 21kG for 45 minutes and the supernatant discarded. This process was repeated once. The pellets were subsequently dissolved in a minimal amount of PBS and each batch transferred to Eppendorf tubes. The solutions were then centrifuged at 16kG for 45 minutes and the supernatant discarded. The pellets were redissolved in PBS and the process repeated once. Finally all the pellets were redissolved in PBS and the aliquots pooled together. The AuNP-CP-1-Tf solutions were filtered through a 0.22 µm PES membrane. The particle concentrations were estimated by UV and particle recovery determined by comparison to the initial stock AuNP Lipoic-MPC-N_3 solution.

Tf – AuNP pPEGMA polymer particle coating

The solutions of AuNP-CP-1 conjugated with Tf (Tf-AuNP-1, Tf-AuNP-2, Tf-AuNP-3) were transferred with a pipette into 1.5 mL Eppendorf tubes. pPEGMA-DBCO was dissolved in isotonic PBS pH 7.4 (33.9 mg/mL). Twenty-six µL of the pPEGMA-DBCO stock solution (882 µg, 41 nmoles, 100 eq. per AuNP) was added to each batch of AuNP and allowed to react for 3 days at 4°C at low speed on an orbital shaker. After 3 days the particles were centrifuged at 21kG for 45 minutes and the supernatant collected. The particles were transferred to 50 mL centrifuged tubes, diluted with isotonic PBS and centrifuged at 21kG for 45 minutes at 4°C. This process was repeated twice. The pellets were afterwards dissolved in minimal amount of PBS and each batch transferred to Eppendorf tubes. The solutions were then centrifuged at

16kG for 45 minutes and the supernatant discarded. The pellets were redissolved in PBS and the process repeated once. Finally all the pellets were redissolved in PBS, the aliquots pooled together and the resultant pPEGMA-conjugated Tf-AuNP solutions were filtered through 0.22 μm PES membrane.

Polymer grafting density to the AuNP was determined by measuring the concentration of polymer in the supernatant by aqueous GPC with 10% methanol and comparing to the polymer stock concentration. The particle concentration was estimated by UV and particle recovery determined by comparison to the initial stock AuNP-Tf solution.

Cloud point analysis of pPEGMA-Tf-AuNP conjugates in DMEM

The stock solutions of pPEGMA-Tf-AuNPs in PBS were diluted 15.5 times with DMEM and their turbidity monitored as a function of temperature. The samples solutions were heated from 20°C to 65°C using a temperature gradient of 1°C/min and UV readings were recorded every 0.3°C at 534 nm.

Cell culture

HeLa cells were cultured in DMEM (Fisher Scientific, Loughborough, UK) supplemented with 10% FBS (Gibco, Fisher Scientific, formally Invitrogen, Paisley, UK) under standard tissue culture conditions (at 37°C, 5% CO_2 in a humidified incubator) and passaged (no greater than 20 times) before reaching 80% confluency. HeLa cells were obtained from ATCC, routinely tested for the absence of mycoplasma and were not cultured in the presence of antibiotics.

Uptake analysis of AuNPs and Transferrin competition

The day before experimentation 275,000 cells were seeded into a glass bottomed imaging dish (MatTek, Ashland, MA, USA) in DMEM containing 10 % FBS and allowed to adhere overnight under standard tissue culture conditions. On the day of experiment, cells were washed three times in imaging medium (phenol red free DMEM containing 20 mM HEPES, [Fisher Scientific, Loughborough, UK] supplemented with 0.1% BSA [Fisher Scientific]) and incubated with $0.85x10^{12}$ AuNPs at a concentration of $4.25x10^{12}$ AuNPs/mL for 2 h in imaging medium at either 33°C or 41°C in a humidified 5% CO_2 incubator. Cells were subsequently washed three times in imaging medium and immediately imaged on a Leica SP5 confocal microscope (488 nm laser, with x63 objective, rastor size of 1024 square giving a pixel size of 151 nm square, images were obtained at 200 Hz, with a line average of three).

For transferrin competition assays, samples were setup as above with the addition (or absence) of 50 µg/mL (625 nM) holo-Tf-Biotin (Sigma Aldrich, Gillingham, UK), in addition to the AuNPs. For the control Tf uptake assay, Tf-Alexa488 (Fisher Scientific) was added at 25 nM in place of AuNPs and treated as above.

Quantification was performed using the method developed by Moody *et al.*[35] In brief, ten individual images were analyzed per sample with the mean of these ten giving a value for an independent experiment. The mean was taken for three individual experiments with the standard error of the mean calculated and plotted. An unpaired two-tailed t-test was used for the comparison of pPEGMA-Tf-AuNP-3 at 41°C and 33°C only. In all other cases, an ANOVA with post-hoc Tukey's test was performed at a significance level of $P<0.05$ was calculated for a comparison of all samples (where pPEGMA-Tf-AuNP-3 at 41°C and 33°C proved significant).

Labelling lysosomes

Cells seeded at 225,000 cells per imaging dish were allowed to adhere for 24 hours before incubation with 100 μg/mL Dextran-Alexa647 for two hours in DMEM containing 10% FBS. Cells were washed three times and incubated overnight in fresh DMEM containing 10% FBS to label lysosomes as described previously.[35]

Uptake time course and colocalization with lysosome

Cell lysosomes were labelled as above. On the day of the experiment, cells were incubated with either pPEGMA-Tf-AuNP-3 at $1.7x10^{12}$ AuNPs per imaging dish (a concentration of $8.5x10^{12}$ AuNPs per mL, thus giving an effective Tf concentration of 42 nM per dish) or with 42 nM Tf-Alexa488 for 2hrs in serum free DMEM containing 0.1% BSA for 2 hrs at 41 °C 5% CO_2 before washing and imaging. This higher concentration facilitated microscopy determination of pPEGMA-Tf-AuNP-3 within the cells, so that a stronger signal could be obtained above background fluorescence. Cells were subsequently reimaged 4 hours and 6 hours post initial incubation via confocal microscopy (488nm and 633nm lasers, with x63 objective, a zoom of 1.73, rastor size of 1024 square giving a pixel size of 139 nm square, equivalent to the resolution limit for this system). Images were obtained at 200Hz, with a line average of three).

Supporting Information. Cloud point analysis, transmission electron microscopy, surface plasmon resonance data, dynamic light scattering and zeta potential measurements. This material is available free of charge via the Internet at http://pubs.acs.org.

AUTHOR INFORMATION

Corresponding Authors

*Cameron Alexander, School of Pharmacy, University of Nottingham, University Park, Nottingham, UK. E-mail: Cameron.alexander@nottingham.ac.uk; Arwyn T Jones, Cardiff School of Pharmacy and Pharmaceutical Sciences, Cardiff University, Cardiff, Wales. E-mail: jonesat@cardiff.ac.uk., Stefano Salmaso, Department of Pharmaceutical and Pharmacological Sciences, University of Padova, Padova, Italy. E-mail: Stefano.salmaso@unipd.it

Present Addresses

Johannes Magnusson, CytRx Drug Discovery Branch, Engesserstr. 4, 79108 Freiburg, Germany. Paul Moody, Oxford Nanopore Technologies, Oxford Science Park, Oxford OX4 4GA, UK.

Author Contributions

# ES and JPM contributed equally to this manuscript. ES, JPM, FM, CB, CC and PJM performed the experiments, SS, PC, GM, PB, PW, JA, ATJ and CA contributed to study design and supervised the research. JPM, ES, ATJ and CA wrote the paper: all authors have given approval to the final version of the manuscript.

Conflict of interest disclosure

The authors declare no competing financial interest.

ACKNOWLEDGMENTS

We thank EPSRC (Grants EP/J021180/1, EP/H005625/1, EP/J021334/1) and the Royal Society (Wolfson Research Merit Award WM150086) for funding this work. Claudia Conte was supported by a Fellowship from Associazione Italiana per la Ricerca sul Cancro (AIRC) co-funded by the European Union (iCARE/Marie Curie 2014). We gratefully acknowledge Drs Darrell Sleep and Karl Nicholls at Albumedix and Dr Hiteshri Makwana for providing thio-transferrin. Paul Cooling, Esme Ireson, Tom Booth and Christine Grainger-Boultby are thanked for expert technical assistance.

Data access statement

All raw data created during this research are openly available from the corresponding author (Cameron.alexander@nottingham.ac.uk) and at the University of Nottingham Research Data Management Repository (https://rdmc.nottingham.ac.uk/) and all analyzed data supporting this study are provided as supplementary information accompanying this paper.

ABBREVIATIONS

AuNP, Gold nanoparticles; TF, Transferrin; DP, Degree of polymerization; RT, Room temperature; Alexa Fluor 488 Sulfodichlorophenol ester (AF488 SDP); HPLC, High performance liquid chromatography; SPR, Surface plasma resonance; GPC, Gel Permeation Chromatography; LCST, Lower critical solution temperature; PAT, polymer aggregation temperature; MPC, 2-Methacryloyloxyethyl phosphorylcholine; DBCO, Dibenzocyclooctyne; DMAP, N.N’-dimethylaminopyridine, DPBS, Dulbecco’s phosphate buffered saline; DMEM, Dulbecco's Modified Eagle Medium.

REFERENCES

(1) Chan, W. C. W., Udugama, B., Kadhiresan, P., Kim, J., Mubareka, S., Weiss, P. S., and Parak, W. J. (2016) Patients, Here Comes More Nanotechnology. *ACS Nano 10*, 8139-8142.
(2) Kim, C. S., Mout, R., Zhao, Y., Yeh, Y.-C., Tang, R., Jeong, Y., Duncan, B., Hardy, J. A., and Rotello, V. M. (2015) Co-Delivery of Protein and Small Molecule Therapeutics Using Nanoparticle-Stabilized Nanocapsules. *Bioconjugate Chemistry 26*, 950-954.
(3) Lim, Y. H., Tiemann, K. M., Heo, G. S., Wagers, P. O., Rezenom, Y. H., Zhang, S., Zhang, F., Youngs, W. J., Hunstad, D. A., and Wooley, K. L. (2015) Preparation and in Vitro Antimicrobial Activity of Silver-Bearing Degradable Polymeric Nanoparticles of Polyphosphoester-block-Poly(L-lactide). *Acs Nano 9*, 1995-2008.
(4) Fan, Z., Shelton, M., Singh, A. K., Senapati, D., Khan, S. A., and Ray, P. C. (2012) Multifunctional Plasmonic Shell-Magnetic Core Nanoparticles for Targeted Diagnostics, Isolation, and Photothermal Destruction of Tumor Cells. *Acs Nano 6*, 1065-1073.
(5) Brazzale, C., Canaparo, R., Racca, L., Foglietta, F., Durando, G., Fantozzi, R., Caliceti, P., Salmaso, S., and Serpe, L. (2016) Enhanced selective sonosensitizing efficacy of ultrasound-based anticancer treatment by targeted gold nanoparticles. *Nanomedicine 11*.
(6) Byzova, N. A., Safenkova, I. V., Slutskaya, E. S., Zherdev, A. V., and Dzantiev, B. B. (2017) Less is More: A Comparison of Antibody–Gold Nanoparticle Conjugates of Different Ratios. *Bioconjugate Chemistry 28*, 2737-2746.
(7) Wilhelm, S., Tavares, A. J., Dai, Q., Ohta, S., Audet, J., Dvorak, H. F., and Chan, W. C. W. (2016) Analysis of nanoparticle delivery to tumours. *Nature Reviews Materials 1*, 16014.
(8) Li, S.-D., and Huang, L. (2008) Pharmacokinetics and Biodistribution of Nanoparticles. *Molecular Pharmaceutics 5*, 496-504.
(9) Yu, T., Hubbard, D., Ray, A., and Ghandehari, H. (2012) In vivo biodistribution and pharmacokinetics of silica nanoparticles as a function of geometry, porosity and surface characteristics. *Journal of Controlled Release 163*, 46-54.
(10) Brown, D. M., Dickson, C., Duncan, P., Al-Attili, F., and Stone, V. (2010) Interaction between nanoparticles and cytokine proteins: impact on protein and particle functionality. *Nanotechnology 21*, 215104.
(11) Lesniak, A., Salvati, A., Santos-Martinez, M. J., Radomski, M. W., Dawson, K. A., and Aberg, C. (2013) Nanoparticle Adhesion to the Cell Membrane and Its Effect on Nanoparticle Uptake Efficiency. *Journal of the American Chemical Society 135*, 1438-1444.
(12) Algar, W. R., Prasuhn, D. E., Stewart, M. H., Jennings, T. L., Blanco-Canosa, J. B., Dawson, P. E., and Medintz, I. L. (2011) The Controlled Display of Biomolecules on Nanoparticles: A Challenge Suited to Bioorthogonal Chemistry. *Bioconjugate Chemistry 22*, 825-858.
(13) Wan, S., Kelly, P. M., Mahon, E., Stockmann, H., Rudd, P. M., Caruso, F., Dawson, K. A., Yan, Y., and Monopoli, M. P. (2015) The "Sweet" Side of the Protein Corona: Effects of Glycosylation on Nanoparticle-Cell Interactions. *Acs Nano 9*, 2157-2166.
(14) Salvati, A., Pitek, A. S., Monopoli, M. P., Prapainop, K., Bombelli, F. B., Hristov, D. R., Kelly, P. M., Aberg, C., Mahon, E., and Dawson, K. A. (2013) Transferrin-functionalized nanoparticles lose their targeting capabilities when a biomolecule corona adsorbs on the surface. *Nature Nanotechnology 8*, 137-143.
(15) Mout, R., Moyano, D. F., Rana, S., and Rotello, V. M. (2012) Surface functionalization of nanoparticles for nanomedicine. *Chemical Society Reviews 41*, 2539-2544.

(16) Choudhury, D., Xavier, P. L., Chaudhari, K., John, R., Dasgupta, A. K., Pradeep, T., and Chakrabarti, G. (2013) Unprecedented inhibition of tubulin polymerization directed by gold nanoparticles inducing cell cycle arrest and apoptosis. *Nanoscale 5*, 4476-4489.

(17) Oh, E., Delehanty, J. B., Sapsford, K. E., Susumu, K., Goswami, R., Blanco-Canosa, J. B., Dawson, P. E., Granek, J., Shoff, M., Zhang, Q., et al. (2011) Cellular Uptake and Fate of PEGylated Gold Nanoparticles Is Dependent on Both Cell-Penetration Peptides and Particle Size. *Acs Nano 5*, 6434-6448.

(18) Kim, C., Agasti, S. S., Zhu, Z. J., Isaacs, L., and Rotello, V. M. (2010) Recognition-mediated activation of therapeutic gold nanoparticles inside living cells. *Nature Chemistry 2*, 962-966.

(19) Jain, S., Hirst, D. G., and O'Sullivan, J. M. (2012) Gold nanoparticles as novel agents for cancer therapy. *Br. J. Radiol. 85*, 101-113.

(20) Duncan, B., Kim, C., and Rotello, V. M. (2010) Gold nanoparticle platforms as drug and biomacromolecule delivery systems. *Journal of Controlled Release 148*, 122-127.

(21) Zhou, Q. Q., Zhang, Y. L., Du, J., Li, Y., Zhou, Y., Fu, Q. X., Zhang, J. G., Wang, X. H., and Zhan, L. S. (2016) Different-Sized Gold Nanoparticle Activator/Antigen Increases Dendritic Cells Accumulation in Liver-Draining Lymph Nodes and CD8+T Cell Responses. *Acs Nano 10*, 2678-2692.

(22) Niikura, K., Kobayashi, K., Takeuchi, C., Fujitani, N., Takahara, S., Ninomiya, T., Hagiwara, K., Mitomo, H., Ito, Y., Osada, Y., et al. (2014) Amphiphilic Gold Nanoparticles Displaying Flexible Bifurcated Ligands as a Carrier for siRNA Delivery into the Cell Cytosol. *Acs Applied Materials & Interfaces 6*, 22146-22154.

(23) Nam, J., La, W. G., Hwang, S., Ha, Y. S., Park, N., Won, N., Jung, S., Bhang, S. H., Ma, Y. J., Cho, Y. M., et al. (2013) pH-Responsive Assembly of Gold Nanoparticles and "Spatiotemporally Concerted" Drug Release for Synergistic Cancer Therapy. *Acs Nano 7*, 3388-3402.

(24) Roy, D., Berguig, G. Y., Ghosn, B., Lane, D. D., Braswell, S., Stayton, P. S., and Convertine, A. J. (2014) Synthesis and characterization of transferrin-targeted chemotherapeutic delivery systems prepared via RAFT copolymerization of high molecular weight PEG macromonomers. *Polymer Chemistry 5*, 1791-1799.

(25) Somani, S., Blatchford, D. R., Millington, O., Stevenson, M. L., and Dufès, C. (2014) Transferrin-bearing polypropylenimine dendrimer for targeted gene delivery to the brain. *Journal of Controlled Release 188*, 78-86.

(26) Jiang, Y. Y., Liu, C., Hong, M. H., Zhu, S. J., and Pei, Y. Y. (2007) Tumor Cell Targeting of Transferrin-PEG-TNF-α Conjugate via a Receptor-Mediated Delivery System: Design, Synthesis, and Biological Evaluation. *Bioconjugate Chem. 18*, 41-49.

(27) Grabowska, A. M., Kircheis, R., Kumari, R., Clarke, P., McKenzie, A., Hughes, J., Mayne, C., Desai, A., Sasso, L., Watson, S. A., et al. (2015) Systemic in vivo delivery of siRNA to tumours using combination of polyethyleneimine and transferrin-polyethyleneimine conjugates. *Biomaterials Science 3*, 1439-1448.

(28) Soliman, M., Nasanit, R., Abulateefeh, S. R., Allen, S., Davies, M. C., Briggs, S. S., Seymour, L. W., Preece, J. A., Grabowska, A. M., Watson, S. A., et al. (2012) Multicomponent Synthetic Polymers with Viral-Mimetic Chemistry for Nucleic Acid Delivery. *Molecular Pharmaceutics 9*, 1-13.

(29) Frazier, N., and Ghandehari, H. (2015) Hyperthermia approaches for enhanced delivery of nanomedicines to solid tumors. *Biotechnology and Bioengineering 112*, 1967-1983.

(30) Magnusson, J. P., Khan, A., Pasparakis, G., Saeed, A. O., Wang, W., and Alexander, C. (2008) Ion-Sensitive "Isothermal" Responsive Polymers Prepared in Water. *J. Am. Chem. Soc. 130*, 10852-10853.
(31) Cepraga, C., Favier, A., Lerouge, F., Alcouffe, P., Chamignon, C., Lanoe, P.-H., Monnereau, C., Marotte, S., Ben Daoud, E., Marvel, J., et al. (2016) Fluorescent gold nanoparticles with chain-end grafted RAFT copolymers: influence of the polymer molecular weight and type of chromophore. *Polymer Chemistry 7*, 6812-6825.
(32) Boyer, C., Whittaker, M. R., Luzon, M., and Davis, T. P. (2009) Design and Synthesis of Dual Thermoresponsive and Antifouling Hybrid Polymer/Gold Nanoparticles. *Macromolecules 42*, 6917-6926.
(33) Vercauteren, D., Deschout, H., Remaut, K., Engbersen, J. F. J., Jones, A. T., Demeester, J., De Smedt, S. C., and Braeckmans, K. (2011) Dynamic Colocalization Microscopy To Characterize Intracellular Trafficking of Nanomedicines. *Acs Nano 5*, 7874-7884.
(34) Tekle, C., van Deurs, B., Sandvig, K., and Iversen, T. G. (2008) Cellular trafficking of quantum dot-ligand bioconjugates and their induction of changes in normal routing of unconjugated ligands. *Nano Letters 8*, 1858-1865.
(35) Moody, P. R., Sayers, E. J., Magnusson, J. P., Alexander, C., Borri, P., Watson, P., and Jones, A. T. (2015) Receptor Crosslinking: A General Method to Trigger Internalization and Lysosomal Targeting of Therapeutic Receptor:Ligand Complexes. *Molecular Therapy 23*, 1888-1898.
(36) Lu, L., Yuan, L., Yan, J., Tang, C., and Wang, Q. (2016) Development of Core–Shell Nanostructures by In Situ Assembly of Pyridine-Grafted Diblock Copolymer and Transferrin for Drug Delivery Applications. *Biomacromolecules 17*, 2321-2328.
(37) Li, S. H., Amat, D., Peng, Z. L., Vanni, S., Raskin, S., De Angulo, G., Othman, A. M., Graham, R. M., and Leblanc, R. M. (2016) Transferrin conjugated nontoxic carbon dots for doxorubicin delivery to target pediatric brain tumor cells. *Nanoscale 8*, 16662-16669.
(38) Choe, U.-J., Rodriguez, A. R., Lee, B. S., Knowles, S. M., Wu, A. M., Deming, T. J., and Kamei, D. T. (2013) Endocytosis and Intracellular Trafficking Properties of Transferrin-Conjugated Block Copolypeptide Vesicles. *Biomacromolecules 14*, 1458-1464.
(39) Fu, J. Y., Zhang, W., Blatchford, D. R., Tetley, L., McConnell, G., and Dufes, C. (2011) Novel tocotrienol-entrapping vesicles can eradicate solid tumors after intravenous administration. *Journal of Controlled Release 154*, 20-26.
(40) Mastrotto, F., Caliceti, P., Amendola, V., Bersani, S., Magnusson, J. P., Meneghetti, M., Mantovani, G., Alexander, C., and Salmaso, S. (2011) Polymer control of ligand display on gold nanoparticles for multimodal switchable cell targeting. *Chemical Communications 47*, 9846-9848.
(41) Zhang, Q., Re Ko, N., and Kwon Oh, J. (2012) Recent advances in stimuli-responsive degradable block copolymer micelles: synthesis and controlled drug delivery applications. *Chemical Communications 48*, 7542-7552.
(42) Van Butsele, K., Cajot, S., Van Vlierberghe, S., Dubruel, P., Passirani, C., Benoit, J. P., Jerome, R., and Jerome, C. (2009) pH-Responsive Flower-Type Micelles Formed by a Biotinylated Poly(2-vinylpyridine)-block-poly(ethylene oxide)-block-poly(epsilon-caprolactone) Triblock Copolymer. *Advanced Functional Materials 19*, 1416-1425.
(43) Kelly, P. M., Åberg, C., Polo, E., O'Connell, A., Cookman, J., Fallon, J., KrpetićŽeljka, and Dawson, K. A. (2015) Mapping protein binding sites on the biomolecular corona of nanoparticles. *Nat Nano 10*, 472-479.

(44) Mahon, E., Salvati, A., Baldelli Bombelli, F., Lynch, I., and Dawson, K. A. (2012) Designing the nanoparticle–biomolecule interface for "targeting and therapeutic delivery". *Journal of Controlled Release 161*, 164-174.
(45) Monopoli, M. P., Aberg, C., Salvati, A., and Dawson, K. A. (2012) Biomolecular coronas provide the biological identity of nanosized materials. *Nature Nanotechnology 7*, 779-786.
(46) Wang, J., Yuan, S., Zhang, Y., Wu, W., Hu, Y., and Jiang, X. (2016) The effects of poly(zwitterions)s versus poly(ethylene glycol) surface coatings on the biodistribution of protein nanoparticles. *Biomaterials Science 4*, 1351-1360.
(47) Sibarani, J., Takai, M., and Ishihara, K. (2007) Surface modification on microfluidic devices with 2-methacryloyloxyethyl phosphorylcholine polymers for reducing unfavorable protein adsorption. *Colloids Surf B Biointerfaces 54*, 88-93.
(48) Feng, W., Zhu, S., Ishihara, K., and Brash, J. L. (2005) Adsorption of Fibrinogen and Lysozyme on Silicon Grafted with Poly(2-methacryloyloxyethyl Phosphorylcholine) via Surface-Initiated Atom Transfer Radical Polymerization. *Langmuir 21*, 5980-5987.
(49) Abulateefeh, S. R., Spain, S. G., Thurecht, K. J., Aylott, J. W., Chan, W. C., Garnett, M. C., and Alexander, C. (2013) Enhanced uptake of nanoparticle drug carriers via a thermoresponsive shell enhances cytotoxicity in a cancer cell line. *Biomaterials Science 1*, 434-442.
(50) Foralosso, R., Moir, L., Mastrotto, F., Sasso, L., Tchoryk, A., Selo, A., Grabowska, A., Ashford, M. B., Aylott, J., Gellert, P. R., et al. (2017) Control of aggregation temperatures in mixed and blended cytocompatible thermoresponsive block co-polymer nanoparticles. *Soft Matter 13*, 7441-7452.
(51) Dai, Q., Yan, Y., Ang, C.-S., Kempe, K., Kamphuis, M. M. J., Dodds, S. J., and Caruso, F. (2015) Monoclonal Antibody-Functionalized Multilayered Particles: Targeting Cancer Cells in the Presence of Protein Coronas. *ACS Nano 9*, 2876-2885.
(52) Finnis, C. J., Payne, T., Hay, J., Dodsworth, N., Wilkinson, D., Morton, P., Saxton, M. J., Tooth, D. J., Evans, R. W., Goldenberg, H., et al. (2010) High-level production of animal-free recombinant transferrin from Saccharomyces cerevisiae. *Microbial Cell Factories 9*, 87.
(53) Magnusson, J. P., Bersani, S., Salmaso, S., Alexander, C., and Caliceti, P. (2010) In Situ Growth of Side-Chain PEG Polymers from Functionalized Human Growth Hormone. A New Technique for Preparation of Enhanced Protein-Polymer Conjugates. *Bioconjugate Chemistry 21*, 671-678.

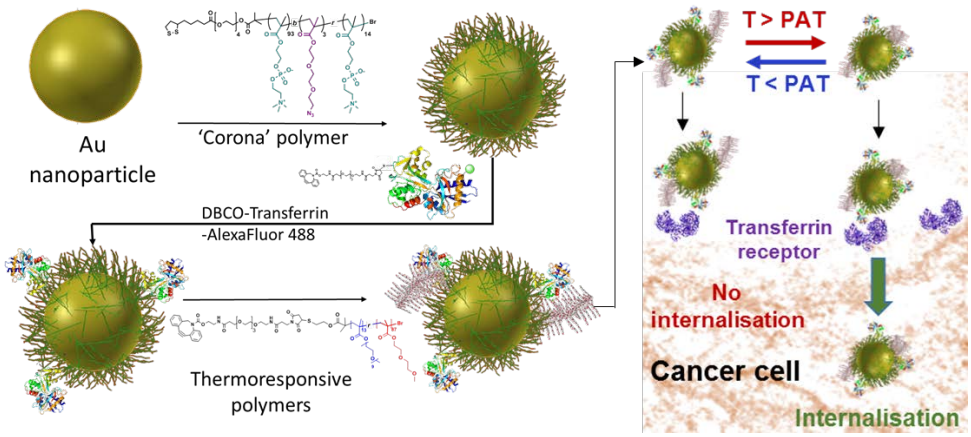

Graphical abstract. Thermoresponsive polymers are used to coat gold nanoparticles with surface-displayed transferrin functionality. Control of transferrin-receptor binding and subsequent internalization into HeLa cells of the gold nanoparticles is modulated by reversible conformational changes of the thermoresponsive polymers.